Deep Time Assessment for the Clive DU PA

Deep Time Assessment for the Clive DU PA Model v1.4

22 November 2015

Prepared by
NEPTUNE AND COMPANY, INC.
1505 15th St, Suite B, Los Alamos, NM 87544

1. Title: Deep Time Assessment for the Clive DU PA		
2. Filename: Deep Time Assessment v1.4.docx		
3. Description: This report describes details of the "deep time" component of the Clive DU PA Model. The "deep time" model addresses long term effects (beyond 10,000 years post-closure) of disposal of DU at the Clive facility.		
	Name	Date
4. Originator	Bruce Crowe, Robert Lee	3 Sep 2015
5. Reviewer	Kate Catlett, Paul Black, Dan Levitt	22 Nov 2015

6. Remarks

3 Jul 2014; R2: Accepted track changes from R1 and added "a" and "b" to identify two Oviatt et al. (1994) references – D. Levitt

30 Jul 2014: Updates and corrections for v1.2. White Paper now at rev 3. — R. Lee and J. Tauxe

27 Aug 2015: Merged "Deep Time Supplemental Analysis. . ." white paper with the Deep Time white paper – R. Lee

03 Sep 2015: Edits- B. Crowe and R. Lee.

09 Sep 2015: Edits – B. Crowe and J. Oviatt

15 Oct 2015: Thorough edits and revisions to add latest GoldSim modeling and model simplification justification. – K. Catlett

1 Nov 2015: Added to Table 1 dose parameters. Revised and added text relevant to latest model (v1.4) consolidation and further CSM clarification.

4 Nov 2015: Added information to section 7, especially regarding dose calcs. K.Catlett and R. Perona

This page is intentionally blank, aside from this statement.

CONTENTS

FIGURES

TABLES

1.0 Deep Time Model Distribution Summary

A summary of parameter values used in the Deep Time Model component of the Clive DU PA Model is provided in Table 1. For the purpose of this white paper, deep time refers to the period between 10 thousand yr to 2.1 million yr; approximately when the progeny of ^{238}U reach secular equilibrium with ^{238}U and peak activity.

For distributions, the following notation is used:

- N(μ, σ, [*min*, *max*]) represents a normal distribution with mean μ and standard deviation σ, and optional *min* and *max* if truncation is needed,
- LN(*GM*, *GSD*, [*min*, *max*]) represents a log-normal distribution with geometric mean GM and geometric standard deviation GSD, and optional *min* and *max* if truncation is needed,
- U([*min*, *max*]) represents a uniform distribution with minimum *min*, and maximum *max*,
- Beta(μ, σ, [*min*, *max*]) represents a generalized beta distribution with mean μ, standard deviation σ, minimum *min*, and maximum *max*, and
- Gamma(μ, σ) represents a gamma distribution with mean μ and standard deviation σ.

Table 1. Summary of distributions for the Deep Time Model container

Model Parameter	Value or Distribution	Units	Reference
DepthEolianDeposition long-term eolian deposition depths	N(μ=72.7, σ=5 min=Small, max=Porosity_Unit4)	cm	Section 7.5
AgeEolianDeposition long-term eolian deposition ages	Beta(μ=13614, σ=263.3,min=13000,max=15000)	yr	Section 7.5
EolianCorrelationFactor correlation between eolian deposition depth and Eolian deposition age	U(0.5,1.0)	—	Section 7.5
LakeDelayTime time at which the intermediate lake calculations are allowed to occur	50,000	yr	Section 4.1
IntermediateLakeDuration length of time that Clive is covered by an intermediate lake	LN(GM=500, GSD=1.5,min=0, max=2500)	yr	Section 7.3

Model Parameter	Value or Distribution	Units	Reference
IntermediateLakeSedimentAmount total depth of sediment laid down by an intermediate lake	LN(GM=2.82, GSD=1.71)	m	Section 7.4
DeepLakeStart time before the end of the 100,000-year climate cycle	LN(GM=14000, GSD=1.2,min=0, max=50000)	yr	Section 7.2
DeepLakeEnd time after the most recent cold peak within the 100,000-year climate cycle	LN(GM=6000, GSD=1.2,min=0, max=50000)	yr	Section 7.2
DeepLakeSedimentationRate rate of the sedimentation during the open water phase of a deep lake	LN(GM=1.2E-4, GSD=1.2)	m/yr	Section 7.4
SiteDispersalArea the area across which the destroyed site is spread	Gamma(mean=24.2332, stdev=11.43731)	Km^2	Section 7.6
IntermediateLakeDepth depth of an intermediate lake at Clive	Beta(μ=30, σ=18,min=0, max=100)	m	Section 7.9
DeepLakeDepth depth of a deep lake at Clive	Beta(μ=150, σ=20,min=100, max=200)	m	Section 7.9
TotalEmbankmentVolume original total volume of the embankment	3,231,556	m^3	Section 7.8
DiffusionLength Diffusion length for the deep time sediments	N(μ=0.5, σ=0.16 min=0.0, max=Large)	m	Section 7.9
external_DCF_modifiers	See table in *ES external DCF modifiers.xlsx* Excel file	—	Section 7.11
DCFs and parameters within the DCFs container	See *Dose Assessment* white paper for parameter values and reference	—	See *Dose Assessment* white paper

Model Parameter	Value or Distribution		Units	Reference
Rn_flux_ratio	Thickness	Rn-222 flux	—	Section 7.10
ratio of Rn-222 flux at different sediment thickness to flux with no overlaying cover	0.001	1.00000		
	0.5	4.392E-1		
	1.0	1.972E-1		
	1.5	8.750E-2		
	2.0	4.000E-2		
	3.0	8.140E-3		
	4.0	1.656E-3		
	5.0	3.371E-4		
	6.0	6.881E-5		
	7.5	1.00E-30		

* "Large" is a very large number, and "Small" is a very small number, as defined by GoldSim.

2.0 Introduction

This white paper provides documentation of the development of parameter values and distributions used for modeling scenarios of the fate of Federal DU Cell waste for the Clive DU PA model in deep time. Data sources are identified and the rationale applied for developing distributions is described. The intent of this white paper is to describe the characteristics and potential processes of deep time and the subsequent effects on waste disposed at the Clive site.

3.0 Deep Time Model Overview

There are two major components of the Clive DU PA Model. The first component addresses quantitative contaminant fate and transport and subsequent dose assessment for 10,000 yr (10 ky). That modeling is based upon projections of current societal conditions into the future and assumes no substantial change in climatic conditions. The second component addresses "deep time" scenario calculations from 10 ky until the time of peak radioactivity. For this PA, peak radioactivity associated with the ingrowth of progeny from ^{238}U occurs at about 2.1 million yr in the future (2.1 My).

The initial Deep Time Models for this site, the Deep Time container of the Clive DU PA v1.0 and v1.2 Models and the Deep Time Supplemental Analysis (DTSA) Model (Clive DU PA Model vDTSA.gsm), addressed DU waste stored above and below the surrounding grade in an embankment. The DTSA model is a standalone model, not directly linked to the PA model. The models assume destruction of the embankment via wave action from a possible return of a lake to the Clive area under future glacial period conditions, and subsequent dispersal of waste. With a review of this modeling, a decision was made by the State of Utah to require Energy*Solutions* to dispose of all DU waste below the surrounding grade, and thus no waste *per se* would be exposed or dispersed upon return of a lake (SC&A, 2015). The only possible mechanisms for dissolution and dispersal of radionuclides would then be associated with radon emanation into the embankment materials and diffusion of dissolved radionuclides upwards. The current PA model (v1.4) retains this assumption, and the 10 ky model and the revised Deep Time Model are now integrated. Additional factors such as eolian (i.e., wind-borne) deposition are also now included. Below is a brief summary of the current conceptual site model (CSM) for the Deep Time Model. These terms and details are explained and discussed further in this report.

- *Time scale of interest:* 10 ky to 2.1 My post-closure.
- *Waste placement:* All DU waste is buried below grade in five waste cells, with a cover embankment.
- *Pluvial* (i.e., caused by increased precipitation) *lake occurrence*: This is driven largely by glacial cycles of cooler and wetter climate conditions. “Deep” lakes occur no more than once per 100-ky cycle. “Intermediate” lakes can occur independent of a deep lake, or as transitory events during the transgressive (rising lake) or regressive (falling lake) phases of a deep lake. An intermediate lake will not occur at the elevation of the Clive site without a return to pluvial conditions.
- *Destruction of embankment:* The embankment will be eroded to the level of the former Lake Bonneville surface (current grade at the time of the first lake return) by wave action and sediment churning during the first return of a deep or intermediate lake. Radionuclides present in the above-grade part of the embankment (as a result of transport processes) will be dispersed and mixed with sediments during active lake erosion across the area of the lake. The waste itself will not be exposed.
- *Release of radionuclides:* Radionuclides in the dispersed sediments will be released to lake water upon destruction of the embankment via diffusion. Radon is allowed to diffuse upward through the sediment when a lake is not present.
- *Fate of radionuclides:* Radionuclides will partition between water and sediments according to their solubility and sorption properties. Insoluble DU will be buried by lake sediments. Radionuclides settle out in sediments after lakes recede.
- *Sedimentation:* Eolian deposition occurs while lake levels are below the Clive site and are incorporated with lake sedimentation rates after the first lake returns. Clastic sedimentation will dominate during formation of intermediate lakes with transitions to carbonate precipitation when there are deep lakes.

The basic Deep Time Model scenario involves projecting the future environment based upon the Pleistocene and Holocene record of climate variations and lake formation in the Bonneville Basin. The conceptual model of the past environment is based upon scientific records (sediment borehole logs, ice cores, deep ocean cores) of the past eight glacial/climate cycles that have lasted approximately 100 ky each. The model considers cycles from the beginning of an interglacial period onwards. In the past 100-ky cycles, after an interglacial period, the average temperature drops and average precipitation increases throughout the glacial cycle, until the relatively cold period (typically an ”ice age”) ends and the next interglacial period begins (Figure 1). The Earth is currently in an interglacial period. The first 10 ky of the Clive DU PA Model is projected under interglacial conditions, and the Deep Time Model calculations include an evaluation of the effect on the Federal DU Cell of future 100-ky glacial cycles for the next 2.1 My. The critical aspect of a glacial period is the potential return of a pluvial lake to the elevation of the Clive site with accompanying lakeshore wave activity that would destroy the Federal DU embankment. Thus, the objective of the Deep Time Model is to assess the potential impact of glacial period pluvial lake events upon and associated with radionuclide release/dispersal from the Federal DU Cell from 10 ky through 2.1 My post-closure.

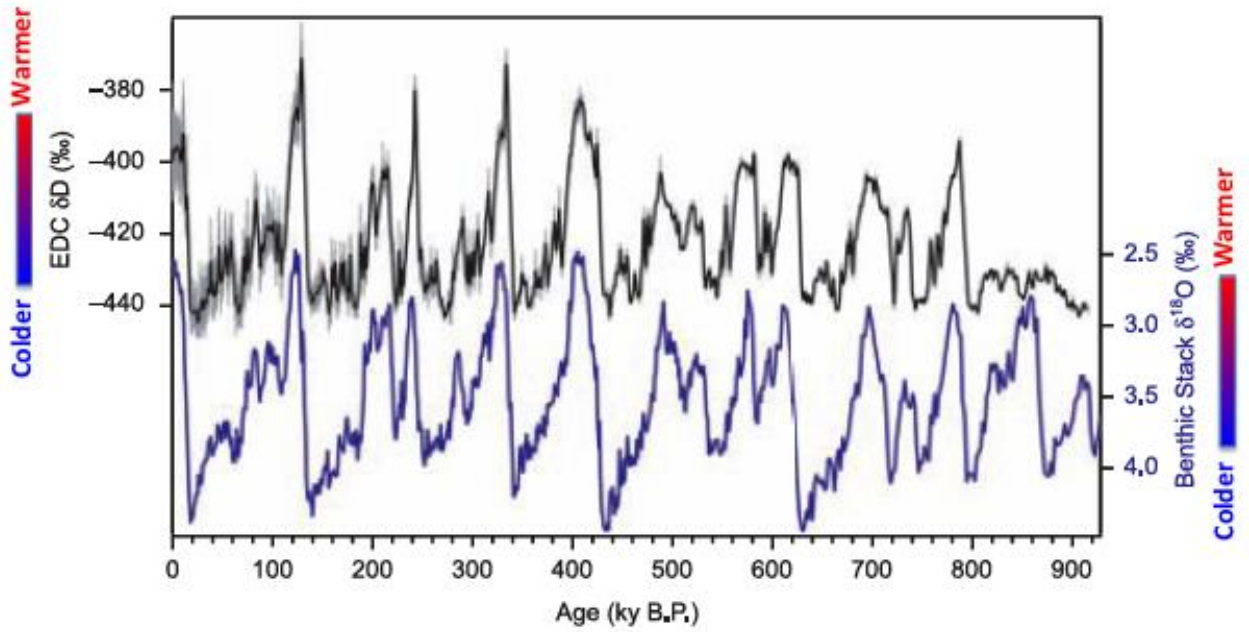

Figure 1. Comparison of delta deuterium (black line) from the European Project for Ice Coring in Antarctica (EPICA) Dome C ice core and benthic (marine) oxygen-18 record (blue line) for the past 900 ky [from Jouzel et al. (2007)]

The approximate historical 100-ky glacial cycles are depicted in Figure 1. The current interglacial period is shown on the left edge of the figure. The last ice age finished between 12,000 and 20,000 yr ago (12 ka and 20 ka, indicated as "ky B.P." in the figure). In the last glacial maximum (represented as a trough on the far-left side of Figure 1), the major Western United States water body Lake Bonneville, which covered much of Utah, reached its maximum extent. Antarctic ice core data as well as benthic marine isotope data (described below) show similar patterns for the past 800 ky. These 100-ky cycles are used as the basis for modeling the return and recurrence of lake events in the Clive area.

The Deep Time Model should be regarded as conceptual and stylized and is not intended as a prediction of expected future conditions at the Clive site. The intent is to estimate potential future radionuclide releases from the remains of the Federal DU Cell, rather than to provide a quantitative, temporally-specific prediction of future conditions, or an assessment of exposure or doses to possible humans. Doses to potential human receptors and the presence and characteristics of human populations in the Clive area during this time period are entirely speculative. When a lake inundates the waste site, there will be no receptors at that location. Additionally, calculation of radiological dose to human at times beyond 10 ky is not required by Utah state regulations (Utah 2015). Instead, these regulations specify a "qualitative" assessment with radionuclide release simulations for this period. Organizations such as the International Atomic Energy Agency (IAEA 2012) have indicated that calculating doses beyond a few hundred yr is not defensible; thus, quantitative dose assessment, particularly subsequent to lake events related to the interglacial cycle, is insupportable from scientific and technical perspectives. However, if the Deep Time Model results such as radon flux are considered in the context of gauging system performance, such results may provide limited insight into the behavior of the

disposal system in deep time. Based on potential future radon fluxes, a rancher dose was calculated in the Deep Time Model to provide a context for the radon flux results.

A "deep" lake is defined here as a large glacial-period lake on the scale of the prehistoric Lake Bonneville (present in the area from about 32 ka to 14 ka). Such lakes have occurred in several of the past 100-ky climate cycles. An "intermediate" lake is defined as a lake that reaches the elevation of Clive (described further below). These lakes are assumed to occur in the transgressive and regressive phases of a deep lake, but evidence of such lakes is difficult to identify and interpret because lake deposits are reworked during their transgressive and regressive lake phases. It is assumed that the first deep or intermediate lake that reaches the elevation of Clive will destroy and disperse the Federal DU Cell embankment via wave action. This dispersal mixes radionuclides with lake sediments. The characteristics of these mixed sediments are dependent upon the duration and intensity of the lakeshore processes (e.g., wave sediment churning, and formation of spits and bars from longshore drift).

Wave action associated with transgressing and regressing intermediate lakes will rework the lake-sediment interface to a depth that is controlled by the dynamics of the wave action. Evidence of wave action and sedimentary processes for past levels of Lake Bonneville is preserved in the area's sedimentary and geomorphic features. This evidence includes paleoshorelines, fan and river deltas, wave-cut cliffs, bayhead barriers and spits (Sack, 1999; Schofield et al., 2004; Nelson, 2012). The most relevant lake features from the geologic record are paleoshorelines. Schofield et al. (2004) divide Lake Bonneville shorelines into erosion-dominated and deposition-dominated. The elevation difference between shoreline bench deposits and shoreline fronts from these studies provides a time-integrated analog for the dynamics of wave action during shoreline transgressions and regressions (see Figure 3 in Schofield et al. 2004). These elevation differences are about 90 cm for erosion-dominated shorelines and 40 to 65 cm for deposition-dominated shorelines. Thus, the process of wave action is assumed to remove approximately the same thickness of sediment (0.5 to 1 m) as the residual embankment thickness (<1 m).

Any periods in which a lake does not exist are assumed to experience eolian (i.e., wind-borne) deposition. Although some removal of embankment materials and sediment via wave action is expected, this is not modeled explicitly. Instead, these effects are assumed to be relatively small compared to eolian and lake deposition effects, and are assumed to have roughly a net zero effect on overall sedimentation before and after the return of an intermediate or deep lake (remaining embankment thickness is about 0.5 m and removal depth is about 0.5 m). The current model thus explicitly considers eolian and lake deposition only as contributors to sedimentation thickness.

Other major geologic or climatic events could also occur in the next 2.1 My. Events such as major meteorite impacts, and volcanic activity such as eruptions associated with the Yellowstone Caldera could also be considered. Such future catastrophic events are often screened from consideration in PAs on the basis of a low probability of occurrence and/or limited consequences. In this case, a major meteorite impact and a future volcanic eruption at Yellowstone were not screened. Instead, the impacts of these events are considered to be so catastrophic on a global scale that their effects would far outweigh any potential radionuclide releases from the Federal DU Cell. The same applies to major climate changes outside of those associated with glacial cycles, although impacts of anthropogenic climate change on future lake events are partially considered here.

4.0 Background on Pluvial Lake Formation in the Bonneville Basin

4.1 Long-term Climate

Large-scale climatic fluctuations over the last 2.6 My (the Quaternary Period, the current and most recent of the three periods of the Cenozoic as defined in the geologic time scale; http://www.geosociety.org/science/timescale/) have been studied extensively in order to understand the mechanisms underlying those changes (Hays et al., 1976, Berger, 1988, Paillard, 2001, Berger and Loutre, 2002). These climatic signals have been observed in marine sediments (Lisiekcki and Raymo, 2005), land records (Oviatt et al., 1999), and ice cores (Jouzel et al., 2007). These large-scale fluctuations in climate have resulted in glacial and interglacial cycles, which have waxed and waned throughout the Quaternary Period. The causes of the onset of the last major northern hemisphere glacial cycles 2.6 million yr ago (Ma) remain uncertain, but several studies suggest that the closing of the Isthmus of Panama caused a marked reorganization of ocean circulation patterns that resulted in continental glaciation (Haug and Tiedemann, 1998, Driscoll and Haug, 1998). Future glacial events are likely to be caused by a combination of the Earth's orbital parameters as well as increases in freshwater inputs to the world's oceans resulting in a disruption to oceanic thermohaline circulation (Driscoll and Haug, 1998).

Changes in the periodicity of glacial cycles have been linked to variations in Earth's orbit around the Sun. These variations were described by the Serbian scientist Milutin Milankovitch in the early 1900s, and are based upon changes that occur due to the eccentricity (i.e., orbital shape) of Earth's orbit every 100-ky, the obliquity (i.e., axial tilt) of Earth's axis every 41 ky, and the precession of the equinoxes (or solstices) (i.e., wobbling of the Earth on its axis) every 21 ky (Berger, 1988). For the first 2 My of the Pleistocene (the first major Epoch of the Quaternary Period), Northern Hemispheric glacial cycles occurred every 41 ky, while the last million yr have indicated glacial cycles occurring every 100-ky, with strong cyclicity in solar radiation every 23 ky (Berger and Loutre, 2002; Paillard, 2006). The shift from shorter to longer cycles is one of the greatest uncertainties associated with utilizing the Milankovitch orbital theory alone to explain the onset of glacial cycles (Paillard, 2006).

Hays et al. (1976), who analyzed changes in the isotopic oxygen ($\delta^{18}O$) composition of deep-sea sediment cores, suggest that major climatic changes have followed both the variations in obliquity and precession through their impact on planetary insolation (i.e., the measure of solar radiation energy received on a given surface area in a given time). In its most common form, oxygen is composed of eight protons and eight neutrons (giving it an atomic weight of 16). This is known as "light" oxygen because a small fraction of oxygen atoms have two extra neutrons and a resulting atomic weight of 18 (^{18}O), which is then known as "heavy" oxygen. ^{18}O is a rare form and is found in only about 1 in 500 atoms of oxygen. The ratio of these two oxygen isotopes has changed over the ages and these changes are a proxy to changing climate that have been used in both ice cores from glaciers and ice caps, and cores of deep sea sediments. Thus, variations in $\delta^{18}O$ reflect changes in oceanic isotopic composition caused by the waxing and waning of Northern Hemispheric ice sheets, and are thus used as a proxy for previous changes in climate (*cf*. Figure 1).

Slightly different external forcing and internal feedback mechanisms can lead to a wide range of responses in terms of the causes of glacial-interglacial cycles. The collection of longer ice core records, such as the European Project for Ice Coring in Antarctica (EPICA) Dome C core located in Antarctica, has highlighted the clear distinctions between different interglacial-glacial cycles (Jouzel et al., 2007). Variation in climatic conditions appears to be sufficient that large differences have occurred in each of the past several 100-ky cycles. At the present time, the EPICA Dome C core is the longest (in duration) Antarctic ice core record available, covering the last 800 ky (Jouzel et al., 2007).

There is considerable uncertainty associated with the number, timing, and recurrence interval of glacially-influenced pluvial lakes in the Bonneville Basin. The 100-ky glacial cycle is roughly correlated with the occurrence of deep lakes (Balch et al. 2005, Davis 1998), and there appear to be smaller, millennial scale ("Dansgaard-Oeschger") cycles within this larger cycle that are not necessarily uniform (Madsen, 2000). For example, the Little Valley lake cycle peaked in elevation at about 135 ka, the Cutler Dam lake cycle peaked about 65 ka, and the Bonneville lake cycle peaked about 18 ka (Machette et al., 1992).

Many studies highlight the importance of past atmospheric composition in the dynamics of glaciations across the Northern Hemisphere, in addition to orbital influences (Masson-Delmotte et al., 2010; Clark et al., 2009; Paillard, 2006). Carbon dioxide (CO_2) is a well-known influence on the atmospheric "greenhouse effect" (i.e. warming due to trapping of solar heat), and is a globally well-mixed gas in the atmosphere due to its long lifetime. Therefore, measurements of this gas in Antarctic ice are globally representative and provide long-term data important for understanding past climatic changes. Direct measurement of CO_2 trapped in the EPICA Dome C core indicates that atmospheric CO_2 concentrations decreased during glacial periods due to greater storage in the deep ocean, thereby causing cooler temperatures from a reduction of the atmosphere's greenhouse effect (EPICA, 2004). Warmer temperatures resulting from elevated concentrations of CO_2 released from the ocean contribute to further warming and could support hypotheses of rapid wasting at the end of glacial events (Hays et al., 1976). Earlier interglacial events (prior to 420 ka), however, are thought to have been cooler than the most recent interglacial events (since 420 ka) (Masson-Delmotte et al., 2010).

The predicted effect of anthropogenic CO_2 on glacial cycles has evolved over time. For example, Berger and Loutre (2002) conducted simulations including orbital forcing (i.e., cycles largely driven by orbital variables) coupled with insolation and CO_2 variations over the next 100-ky. Their results indicated that the current interglacial period could last another 50 ky with the next glacial maximum occurring about 100 ky from now. The scientific record (*cf*. Figure 1) supports this pattern of variability across the 100-ky glacial cycles. Berger and Loutre (2002) effectively indicate that the current 100-ky cycle will not be as glacially intense as some of the previous cycles. They also quote J. Murray Mitchell (Kukla et al, 1972, p. 436) who predicts that "the net impact of human activities on climate of the future decades and centuries is quite likely to be one of warming and therefore favorable to the perpetuation of the present interglacial." Archer and Ganopolski (2005) conducted simulations suggesting that the combination of relatively weak orbital forcing and the long atmospheric lifetime of carbon release from fossil fuel and methane hydrate deposits could prevent glaciation for the next 500 ky over two glacial cycle eccentricity minima. Cochelin et al. (2006) used a paleoclimate model to simulate the next glacial inception under orbital and atmospheric CO_2 forcings. Three scenarios were modeled: an impending

glacial inception under low CO_2 levels; a glacial inception in 50 ky for CO_2 levels of 280 to 290 ppm; and no glacial inception for the next 100-ky for CO_2 levels of 300 ppm or higher. Tzedakis et al. (2012a) defined interglacial periods as episodes where global climate is incompatible with the wide global extent of glaciers, and examined differences in such interglacial durations over the last 800 ky. They noted that the onset of interglacials occurs within 2 ky of the boreal summer insolation maximum consistent with Milankovitch forcing, whereas the end of interglacials does not occur consistently on a similar part of the insolation curve. Reduction in summer insolation is identified as a primary trigger for glacial inception, but multiple other feedbacks including atmospheric CO_2 concentrations combine to modify the timing of glacial inception. They further recognized two main groups for mean duration of interglacials: 13 ± 3 ky and 28 ± 2 ky. In a related paper, Tzedakis et al. (2012b) suggest that the end of the current interglacial could occur within the next 1,500 yr if atmospheric CO_2 concentrations were reduced to about 240 ppm, but no glacial inception is projected to occur at current atmospheric CO_2 concentrations of 400 ppm, consistent with the conclusions of Archer and Granopolski (2005).

Jansen et al. (2007) in Chapter 6 of the fourth assessment report of the Intergovernmental Panel on Climate Change (IPCC) concluded that "it is very unlikely that the Earth would naturally enter another ice age for at least 30 ky." These conclusions were updated and strengthened in Chapter 5 of the fifth IPCC assessment report (Masson-Delmotte et al., 2013).

> "Since orbital forcing can be accurately calculated for the future…, efforts can be made to predict the onset of the next glacial period. However, the glaciation threshold depends not only on insolation but also on the atmospheric CO_2 concentration… Models of different complexity have been used to investigate the response to orbital forcing in the future for a range of atmospheric CO_2 levels. These results consistently show that a glacial inception is not expected to happen within the next approximate 50 ky if either atmospheric CO_2 concentration remains above 300 ppm or cumulative carbon emissions exceed 1000 PgC [petagrams of carbon—one petagram is 10^{15} g]. Only if atmospheric CO_2 content was [sic] below the pre-industrial level would a glaciation be possible under present orbital configuration… Simulations with climate–carbon cycle models show multi-millennial lifetime of the anthropogenic CO_2 in the atmosphere… Even for the lowest [emissions] scenario, atmospheric CO_2 concentrations will exceed 300 ppm until the year 3000. It is therefore *virtually certain* [i.e., a greater-than 99% probability] that orbital forcing will not trigger a glacial inception before the end of the next millennium."

Current CO_2 levels are approximately 400 ppm (http://co2now.org/images/stories/data/co2-mlo-monthly-noaa-esrl.pdf), and have been steadily rising over the past 150 yr due to anthropogenic sources. Preindustrial levels of CO_2 were about 280 ppm, and CO_2 levels associated with glacial periods tend to be about 240 ppm (Tzedakis et al., 2012b). It would require major reductions in CO_2 emissions worldwide in order to return to preindustrial levels, and/or engineering solutions (e.g., "scrubbing" on a massive scale) to remove CO_2 from the atmosphere so that pre-industrial levels are attained. However, the Clive DU PA Model projects current knowledge as a fundamental assumption, therefore it is assumed here that no major anthropogenic CO_2-reduction interventions will occur, and that CO_2 levels will continue to rise, or at least will not attain preindustrial levels within the next 50 ky or longer.

The Bonneville basin watershed is large and integrates runoff from the eastern Great Basin and transition region of the Colorado plateau. Long-term changes in evaporation and precipitation over a large region are required to sustain rising of a lake to the Clive elevation. These conditions may be expected to occur only with a return to glacial conditions given climate model forecasts of increased aridity for the southwest United States. Climate change risks to municipal water supplies in Utah have been modeled using watershed hydrology models that explore temporal changes in average conditions (temperature, precipitation, runoff), and severe drought and water supply scenarios (e.g., the Salt Lake City Department of Public Utilities, Bardsley et al., 2013). These types of studies are both prudent and timely, but future projections of decade scale data are highly uncertain. Indeed, projection of the global climate change model results to regional models has been a developing topic in the succession of IPCC reports. Warming temperatures associated with anthropogenic climate effects will likely have appreciable impacts on the Southwestern United States, but current drought projections do not exceed paleoclimate records of droughts over the last two millennia (Woodhouse et al., 2010; Morgan and Pomerleau, 2012). Multi-model ensemble studies of future climate projections from 16 global climate models show both decreases and increases in streamflow projections for the upper Colorado River Basin (Harding et al., 2012). Cook et al. (2010) suggest caution in projecting climate model projections for the arid Southwest.

Regardless, the weight of evidence reviewed and summarized in the sequence of IPCC reports is considered to be substantive and persuasive, and this information supports the current modeling. It is assumed that CO_2 levels will continue to rise for the foreseeable future, or will not decrease below pre-industrial levels. It is also assumed that the IPCC and associated climate projection studies are valid, with a high degree of confidence, including their conclusion that the inception of the next glacial period will probably not occur for at least 50 ky.

The following sub-sections present an overall background on past events in the Bonneville basin that are driven by major shifts in climate, and that are presumed to occur in the distant future as well.

4.2 Prehistorical Deep Lake Cycles

The Bonneville basin is the largest drainage basin in the Great Basin of the Western United States. It is a hydrologically closed basin of over 134,000 km^2, and has previously been occupied by deep pluvial lakes. Pluvial lakes typically form when warm air from arid regions meets chilled air from glaciers, creating cloudy, cool, rainy weather beyond the terminus of the glacier. The increase in rainfall and moisture can fill the drainage basin, forming a lake. This kind of climate was evident during the last glacial period in North America, and resulted in more precipitation than evaporation, hence the rise of Lake Bonneville.

Numerous studies have investigated previous lake cycles in the Bonneville Basin. These include studies of Lake Bonneville shoreline geomorphology (Currey et al., 1984), palynological (i.e., pollen) studies of deep boreholes (Davis, 1998), and studies of the geochemistry of deep-water lacustrine depositional sequences (Eardley et al., 1973; Oviatt et al., 1999, Balch et al., 2005). Analysis of these sediment cores can be used to help understand previous lake levels and characteristics as well as establish the approximate age of previous lake cycles (e.g., Oviatt et al., 1999).

Oviatt et al. (1999) analyzed hydrolysate amino acid enantiomers for aspartic acid, which is abundant in ostracode protein. Ostracodes are small crustaceans that are useful indicators of paleo-environments because of their widespread occurrence and because they are easily preserved. Ostracodes are highly sensitive to water salinity and other limnologic changes. Therefore, portions of sediment cores that contain ostracodes indicate fresher, and hence probably deeper, lake conditions than the modern Great Salt Lake (Oviatt et al., 1999). An important exception to the deep lake interpretation inferred from the presence of ostracodes is wetland/spring discharge areas. While wetland sites contain abundant ostracodes, the sites can generally be discriminated from deep lake carbonates by their lithology and stratigraphic position of the former within transgressive and regressive lake cycles. To establish the approximate timing of previous lake cycles, Oviatt et al. (1999) examined sediments from the Burmester sediment core originally collected in the early 1970s near Burmester, Utah (Eardley et al., 1973). Burmester is approximately 65 km east of Clive on the southern edge of the Great Salt Lake, at an elevation of 1286 m above mean sea level (amsl). The Clive area has an elevation of 1307 m amsl. Oviatt has also collected sediment data from Knolls (to the west of Clive) and at Clive itself (described further below). These data are largely consistent with the more recent layers from Burmester, indicating similar sedimentation processes at work at least during these time periods.

Data from the 307-m Burmester core suggest that a total of four deep-lake cycles occurred during the past 780 ky (Table 2.). Oviatt et al. (1999) found that the four lake cycles correlated with marine $\delta^{18}O$ stages 2 (Bonneville lake cycle: ~24 to 12 ky), 6 (Little Valley lake cycle: ~186 to 128 ky), 12 (Pokes Point lake cycle: ~478 to 423 ky), and 16 (Lava Creek lake cycle: ~659 to 620 ky).

Oxygen isotope stages are alternating warm and cool periods in the Earth's paleoclimate which are deduced from oxygen isotope data (Figure 2). These stages suggest that deep pluvial lake formation in the Bonneville basin occurred in the past only during the most extensive Northern Hemisphere glaciations. There are many interacting mechanisms that could control or 'force' glaciation and deglaciation. For example, Oviatt (1997) and Asmerom et al. (2010) suggested that these extensive glaciations were controlled by the mean position of storm tracks throughout the Pleistocene, which were in turn controlled by the size and shape of the ice sheets. Other glaciation forcing mechanisms have been suggested. The review by Ruddiman (2006) suggests that insolation changes due to orbital tilt and precession, greenhouse gas concentrations, changes in Pacific Ocean circulation, and possibly other interacting mechanisms could contribute to glaciation and deglaciation cycles in North America, and thus pluvial lake existence and size. Lyle et al. (2012) suggests that lake levels in the Pleistocene western US were influenced by stronger spring/summer precipitation fed by tropical Pacific air masses, rather than higher numbers of westerly winter storms.

Balch et al (2005) conducted a more recent detailed study on ostracode fossils in Great Salt Lake sediment (i.e., under the lake). Other fossil invertebrates were also used as paleoecological indicators in this study. Both brine shrimp and brine fly fossils are indicators of hypersaline environments because they have a much higher salinity tolerance than most other invertebrates. This study's findings were consistent with Oviatt et al.'s (1999) later cycles, but as the core was not as deep the findings are not as useful for the present purpose as the Burmester data. The Burmester core data are more germane to the present modeling effort because they represent a relatively long time period in which to establish the occurrence of pluvial lakes in the region.

Table 2. Lake cycles in the Bonneville basin during the last 700 ky[1]

Lake Cycle	Approximate Age[2]	Maximum Elevation	Lake Level Influences
Great Salt Lake (current level)	present	1284 m (4212 ft) in 1873	Interglacial climate; human intervention
Bonneville (Gilbert Episode)	11.6 ka	1295 m (4250 ft)	Beginning of interglacial climate;
Bonneville (Provo Shoreline)	17.4 to 15.0 ka	1445 m (4740 ft)	Glacial climate; new threshold at Red Rock Pass, Idaho (natural dam collapse)
Bonneville (Bonneville Shoreline)	18.0 ka	1552 m (5090 ft)	Glacial climate; threshold at Zenda near Red Rock Pass, Idaho
Bonneville Transgression	~30 to 18.0 ka		Glacial climate
Bonneville (Stansbury Shoreline)	26 to 24 ka	1372 m (4500 ft)	Glacial climate; transgressive phase of Lake Bonneville
Cutler Dam	~80 to 40 ka	<1380 m (<4525 ft)	Glacial climate
Little Valley	~128 to 186 ka	1490 m (4887 ft)	Glacial climate
Pokes Point	417 to 478 ka	1428 m (4684 ft)	Glacial climate
Lava Creek	~620 to 659 ka	1420 m (4658 ft)	Glacial climate

Elevations are not corrected for isostatic variations.
[1] Note the various levels of the last major lake cycle, Lake Bonneville.
[2] Approximate ages derived from Currey, et al. (1984) Link et al. (1999) and Oviatt et al. (1999). Bonneville cycle approximate age presented as calibrated yr.

However, note that there is considerable uncertainty associated with the number, timing, and recurrence interval of lakes in the Bonneville Basin. The 100-ky glacial cycle is roughly correlated with the occurrence of deep lakes (Balch et al., 2005; Davis, 1998), and there appear to be smaller, millennial-scale cycles within this larger cycle that are not necessarily uniform (Machette et al., 1992; Madsen, 2000). It is likely that intermediate lakes have also occurred in each glacial period, but the shorelines have been destroyed by later lakes. Sediment mixing that occurs during lake formation can also mask the existence of previous intermediate lakes. Thus, it is impossible to have complete confidence in historical lake formation characteristics and formation.

Lake Bonneville is the last major deep lake cycle that took place in the Bonneville basin and is widely described in the literature (Hart et al., 2004; Oviatt and Nash, 1989; Oviatt et al., 1994a, 1999). Lake Bonneville was a pluvial lake that began forming approximately 28 to 30 ka, forming various shorelines throughout its existence and covering over 51,000 km^2 at its highest level (Matsubara and Howard, 2009).

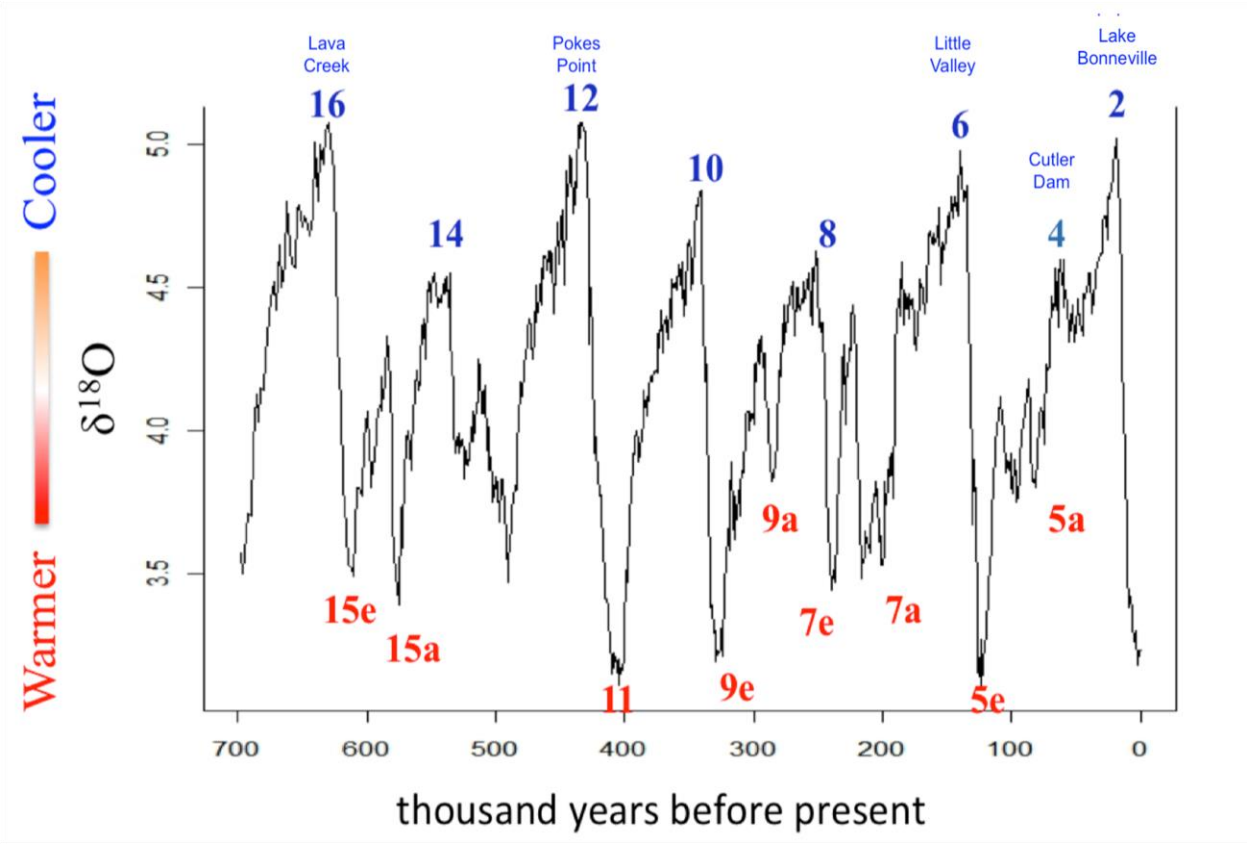

Figure 2. Benthic oxygen isotope record for 700 ka (from Lisiecki and Raymo, 2005)[1]

Most studies indicate that the high-stand (i.e., the highest level reached) of the lake at the Zenda threshold (1,552 m amsl), located north of Red Rock Pass, occurred approximately 18.0 ka. The high-stand of the lake was followed by an abrupt drop in lake level due to the catastrophic failure (landslide) of a natural dam composed of unconsolidated material at approximately 17.4 ka. As a result of this flood, the lake dropped to a level of 1,430 m amsl, called the Provo level (Miller et al. 2013). The Provo level is the maximum level that any future deep lake is likely to reach without major regional tectonic changes (Currey et al., 1984; Oviatt et al., 1999).

A more recent study (Miller et al., 2013), using radiocarbon dating for Provo shoreline gastropod deposits, estimates that the dam collapse and Bonneville flood event occurred between 18.0 and 18.5 ka, and therefore the high-stand may have occurred earlier. However, Miller et al. (2013) indicate that "uncertainties in [gastropod] shell ages may be as large as thousands of yr, and the major shorelines of Lake Bonneville and the Bonneville flood require more work to establish a reliable chronology." The lake regressed rapidly during the last deglaciation, then increased again to form the Gilbert episode ~ 11.6 ka, which remained below the elevation of Clive (Oviatt, 2014). The lake then receded to levels of the current Great Salt Lake at approximately 10 ka for the remainder of the Holocene Epoch.

[1]Red (warm periods) and blue (cool periods) values correspond to marine isotope stages based upon Lisiecki and Raymo (2005). Lake stages identified by Oviatt et al. (1999) are also included in blue text.

Glacial cycles can be discerned in Figure 2 by considering each cycle from the beginning of the interglacial period and ending each cycle at the peaks that correspond to deep lake occurrence. Using this approach, the current glacial cycle started around 12 ka, Lake Bonneville occurred at the end of the last complete cycle, and Cutler Dam occurred in the middle of the last 100-ky cycle. The previous 100-ky cycle resulted in the Little Valley lake. The Pokes Point lake occurred five cycles ago, and The Lava Creek lake seven cycles ago. These deep lakes have been identified in sediment cores and in shorelines around the Bonneville Basin. However, it is likely that many more shallow lakes have also occurred in each glacial period, but the shorelines have been destroyed by subsequent deeper lakes.

The types of sediment resulting from the formation and long-term presence of lakes in the Bonneville basin are diverse and can be divided into three components (Schnurrenberger et al., 2003): 1) chemical sediment (inorganic materials formed within the lake), 2) biogenic sediment (fossil remains of former living organisms), and 3) terrigenous or clastic sediments (grains and clasts that are mechanically and chemically fragmented from existing material, transported and deposited by sedimentary processes). A fourth type of associated sediment, not formed by lakes, includes eolian deposits consisting of windblown grains of sand, silt or dust (i.e., loess). These deposits can locally be interbedded with lake sediments and may be affected by soil-forming processes (i.e., pedogenesis) during prolonged periods of subaerial exposure. All four types of sediments can be intermixed by lake-wave action or bioturbation, and deposited as clastic sediments during transgressive and regressive lake cycles.

There is considerable uncertainty in the number of lakes, particularly lakes of intermediate size that might have existed in the Bonneville basin. However, the main focus of the Deep Time Model is to evaluate the presence of lakes that inundate Clive in future glacial cycles, and to approximately match the net sedimentation of the past glacial cycles. In order to inform the potential for radionuclide releases, the high-level, conceptual modeling of lake cycles that was conducted here did not assume any particular mechanism of glaciation and deglaciation. For example, the modeling simply assumed a 100-ky cycle, regardless of the mechanism. The model addresses deep lakes by allowing them to return in some glacial cycles, and by allowing intermediate lakes to occur as part of the transgressive and regressive phases of deep lake development.

4.3 Shallow and Intermediate Lake Cycles

The current Great Salt Lake is an example of a shallow lake, as is the reinterpreted Gilbert episode lake that has been shown to have not reached the elevation of the Clive site (Oviatt, 2014, contrasted with the map of Currey et al., 1984). The specific depths of lakes are not important in the Deep Time Model, aside from calculations with regard to lake chemistry and dominant processes of sedimentation. Under current climate conditions, only shallow lakes will occur. Under future climate conditions, some glacial cycles will produce deep lakes in the Bonneville basin, and intermediate lakes will occur during the transgressive and regressive phases of deep lakes, or during glacial cycles that do not produce deep lakes. The approximate timing of the return of the first intermediate lake is important in the Deep Time Model, because it is assumed that the Federal DU Cell embankment is destroyed upon the occurrence of the first intermediate lake.

A key assumption of the Deep Time Model, based upon core sediment studies, is that the net depositional rate of deep lakes is lower than the sediment depositional rate for intermediate lakes. The conceptual basis for this assumption is that sedimentation rates are dependent on basin location, presence or absence of fluvial deposition, wave dynamics, availability of local sediment sources, slope, water chemistry and biological activity. Biogenic carbonate deposition is likely to occur under a wide range of lake conditions, but the ratio of carbonate deposition to clastic sedimentation will increase as the lake deepens because of the reduction in sedimentary influx with increased distance from shoreline processes and decreased wave activity.

There are recognized trends in carbonate mineralogy that can be correlated with lake volume and indirectly lake depth (cf., Oviatt, 2002; Oviatt et al., 1994b; Benson et al., 2011). The transitions from low-magnesium calcite to high-magnesium calcite to aragonite generally reflect increasing lake salinity and increasing magnesium concentration, which occurs with decreasing lake volume. Similarly, for a hydrologically closed pluvial lake system, the relative concentration of total inorganic carbon should typically decrease as lake size increases. The $\delta^{18}O$ of deposited carbonate can be correlated with rising lake levels because of the interplay between the $\delta^{18}O$ value of river discharge entering a lake and the $\delta^{18}O$ value of water vapor exiting the system via evaporation (Benson, et al., 2011). The mineralogy and isotopic composition of carbonate composition can be obtained from sediment cores. Interpretation of the data is complicated by multiple processes, including: local groundwater discharge; introduction of glacial rock flour; and, reworking of lake sediments during transgressive and regressive lake cycles.

Intermediate lake events are known to have occurred in the Clive area. These are documented in Table 3 (C.G. Oviatt, Professor of Geology, Kansas State University, personal communication December 2010, January 2011, and various email communication referred to as "C.G. Oviatt, personal communication."). These events are evident from a pit wall interpretation at the Clive site (Appendix A; C.G. Oviatt, unpublished data) as well as at the ostracode and snail record present in the Knolls sediment core (12 km west of Clive near the Bonneville Salt Flats; Appendix B; C.G. Oviatt, unpublished data). In 1985 Lake Bonneville sediments were described and measured in a pit wall during early development of the Clive disposal facility (Oviatt, 1985). Lake sediments of intermediate and deep lakes were briefly studied during field studies at Clive in the winter of 2014 (Neptune, 2015a). These studies confirmed:

1. The pit walls described by C.G. Oviatt in 1985 have been removed during quarrying and/or disposal operations at the Clive site.
2. Soil-modified eolian silt (mean thickness 73 cm) was observed in the upper part of quarry walls throughout the Clive site.
3. The stratigraphy of sediments of Lake Bonneville in modern quarry-wall exposures are consistent with the 1985 pit wall interpretations (Appendix A).
4. Quarry-wall deposits of gravel and sand at the Clive site contain distinctive volcanic clasts of black andesite derived from the Grayback Hills north of Clive. These deposits are part of the transgressive Lake Bonneville sedimentary sequence.
5. Pre-Lake Bonneville lake sediments with interbedded-soils and eolian sands were observed in one deep quarry wall at the north end of the Clive site. These sediments are consistent with the 1985 pit-wall interpretations but the new exposures were insufficiently studied to established sediment correlations and the deposition chronology.

Stratigraphic correlations between 1985 studies and the new field studies (Neptune, 2015a) are shown in Appendix A.

From the Clive pit wall interpretation, it is presumed that at least three intermediate lake cycles occurred prior to the Bonneville cycle, although there is uncertainty associated with this estimate. For example, these intermediate cycles could be part of the transgressive phase (i.e., rising lake level) of the Lake Bonneville cycle (C.G. Oviatt, personal communication). By analyzing the Knolls Core interpretation, the Little Valley cycle is present at approximately 16.8 m from the top of the core. Given that the pit wall at Clive was 6.1 m high and does not capture the Little Valley cycle, it is possible that other smaller lake cycles occurred in the Clive region in addition to the three intermediate lake events noted in Table 3 (labeled as Pre-Bonneville Lacustrine Cycles).

There are few data to support the specific number of lakes that might have reached Clive or the rate of sedimentation. There is also uncertainty associated with the particular times that these cycles occur, as age dating (e.g., via radiocarbon dating) has not been performed in the Great Salt Lake area. Most studies examine the degree of lake salinity using fossil records, and are associated with cores that are in or near the Great Salt Lake. For example, Balch et al. (2005; Fig. 6) estimated that there were six "saline/hypersaline" (i.e., shallow to intermediate) lake cycles that occurred between the Lake Bonneville and Little Valley cycles, and approximately that same number between the Little Valley cycle and the maximum age evaluated (300 ky). However, this work does not inform the question of whether these lakes may have reached the elevation of Clive, nor does similar work such as Davis (1998).

It is also possible that intermediate lakes could reach the elevation of Clive under unusual conditions not necessarily associated with a return to a glacial cycle. The areal extent of lakes is not only determined by elevation, but also by local topography, precipitation, temperature, characteristics of inflow and outflow sources, and other factors. For instance, the Great Salt Lake 'spilled' over a 1285-m (4217-ft) amsl topographic barrier to the west of the present lake into the area of the present Great Salt Desert as recently as the 1700s (Currey et al., 1984). This expanded lake was about 15 m lower than the Clive site, and slightly higher than the current surface elevation of the Great Salt Lake.

Precise dating of shorelines for the Great Salt Lake and variants is unfortunately lacking. Radiocarbon dating for the Pyramid Lake area in Nevada indicates that this lake's levels have lowered approximately 35 m from the late Holocene Epoch (3.5 to 2.0 ky) to today (Briggs et al., 2005). Radiocarbon and tree-ring dating to determine lake levels in the Carson Sink area in Nevada indicates that lake elevations have risen approximately 20 m twice in the last 2000 yr (Adams, 2003). It is not possible at this time to interpolate from these studies to the Great Salt Lake area. However, given the lack of empirical evidence that under present climate conditions (as opposed to cooler, wetter conditions) an intermediate lake would reach the Clive site, this condition is not addressed in the Deep Time Model.

Table 3. Lake cycles and sediment thickness from Clive pit wall interpretation (C. G. Oviatt, personal communication) [1]

Lake Cycle	Thickness of Sediment Layer (m)	Depth Below Ground Surface (m)
Soil-modified eolian silt[1]	1.05	1.05
Lake Bonneville Regressive Phase (reworked marl)	0.43	1.48
Lake Bonneville Open Water (white marl)	1.29	2.77
Lake Bonneville Transgressive (littoral facies)	0.76	3.53
Pre-Bonneville Lacustrine Cycle 3 (possible shallow lake)	0.71	4.24
Pre-Bonneville Lacustrine Cycle 2 (possible shallow lake)	0.62	4.86
Pre-Bonneville Lacustrine Cycle 1 (possible shallow lake)	1.14	6.00

[1] The upper sedimentary sequence is no longer interpreted as a Gilbert lake phase (Oviatt, 2014). It is surficial eolian deposits and soils based on recent field studies (Neptune, 2015a). The pit wall described in the 1985 studies has been removed during quarrying and/or disposal operations.

4.4 Sedimentation

During all pluvial lake cycles, evaporites are deposited, as well as carbonates in the form of tufas, marls, and mudstones. These sediments may contain varying components of shells (e.g. of mollusks), and ostracodes (Hart et al., 2004). Terrigenous sedimentation however, accounts for the major thickness of sediment observed throughout the Clive area sediment core record (C.G. Oviatt, personal communication). The geomorphological evidence in the form of depositional and erosional landforms produced at lake shorelines are carved into the landscape in the Bonneville basin and provide examples of the erosional capacity of lake systems over long time periods. Given the difficulty in separating chemical, biogenic, and terrigenous sediment deposits in cores and natural exposures, the estimates reported below are assumed to be representative of cumulative sedimentation from all causes during a lake event.

Brimhall and Merritt (1981) reviewed previous studies that analyzed sediment cores of Utah Lake, a freshwater remnant of Lake Bonneville that formed at approximately 10 ka. They suggest that up to 8.5 m of sediment has accumulated since the genesis of Utah Lake, implying an average sedimentation rate of 0.85 mm/y or 850 mm/ky. Within the Bonneville basin as a whole the major lake cycles resulted in substantial accumulations of sediment based upon the depth of the cores analyzed (e.g., a 110 m core that corresponds to the past 780 ky, or four deep lake cycles [Oviatt et al., 1999]). This accumulation averages about 140 mm/ky. Einsele and Hinderer (1997) indicate that sediment accumulation in the Bonneville basin occurred at a rate of 120 mm/ky during the past 800 ky. The Knolls Core suggests that there has been 16.8 m of sediment formed in the last glacial cycle, or nearly 170 mm/ky.

Interpretations of the Clive pit wall (C.G. Oviatt, unpublished data) indicate that the sedimentation rate at the Clive site for the Lake Bonneville cycle is on the order of 2.75 m over a 17 to 19 ky time period (140 to 160 mm/ky). By contrast, shallow lacustrine cycles that occurred prior to Lake Bonneville (but after the Little Valley cycle) indicate that the amount of sediment deposited during each cycle is approximately 1/3 that of the Bonneville sediment deposited. The timing of these shallow lake cycles is uncertain, however it can be approximated when

comparing the Clive pit wall interpretation to the Knolls Core (C.G. Oviatt, personal communication). The Little Valley lake cycle is exhibited in the Knolls Core at a depth of approximately 17 m, which is roughly 14 m deeper than the beginning of the transgressive phase of the Bonneville lake cycle event noted on the Clive pit wall interpretation. Given the Little Valley event occurred 150 ka, a sedimentation rate can be approximated for the depth between this event and the transgressive phase of the Bonneville cycle of 110 mm/ky.

4.5 Eolian Deposition

Post-Lake Bonneville eolian deposition has occurred and will continue to occur at the Clive site under current conditions. The expected primary mode of eolian deposition at the Clive site is deposition of fine-grained silt from suspension fallout during episodic wind storms. Exceptionally strong surface winds could potentially transport sand-sized material by saltation. Evidence supporting these conclusions include (Neptune, 2015a):

- The presence of soil-modified eolian silt in the upper part of quarry-wall exposures at multiple locations in the Clive site. The presence of these deposits requires continuing eolian activity in the region and long-term maintenance of stable surfaces that promotes preservation of the eolian deposits (suspension fallout) and soil-forming processes.
- Holocene dune deposits of eolian sand and silt in road cut exposures within 0.5 km of the Clive site.
- Active gypsum sand dunes located approximately 13.5 km west of the Clive site.
- Active dune fields in the Lake Bonneville basin west and southwest of the Clive site (Jewell and Nicoll, 2011).

Replicate measurements of the thickness of eolian deposits located in quarry wall exposures in the Clive site are presented in Neptune (2015), and are used below to develop input probability distributions for the Deep Time Model. These deposits are relevant to expected future eolian sedimentation before the first return of an intermediate or deep lake; with the rise of a future lake to the elevation of the Clive site, wave activity will rework the eolian sediments and intermix them with clastic lakeshore sediments.

5.0 Conceptual Overview of Modeling Future Lake Cycles

5.1 Introduction

There is a lack of data and peer-reviewed literature that would allow accurate and precise prediction of the direct effects of future climate change on intermediate and deep lake formation in the Bonneville basin. However, assuming no major changes from prehistorical climate cycles, there is a possibility of another major lake cycle occurring in the Bonneville basin within the next few million yr. Variations in the Earth's orbital parameters in combination with increases in inputs of freshwater into the oceans could lead to another major ice age and could alter long-term climatic patterns in the Bonneville basin, resulting in deep lake formation. The Clive site might be subjected to deep lake formation in the future, unless anthropogenic effects on atmospheric CO_2 concentrations cause major long-term changes in glacial cycles and climatic patterns.

An overview of the Deep-Time CSM was presented at the beginning of this report. The basic intent of the Deep Time Model is to allow a lake to exist that is sufficiently large that the above-ground embankment of the Federal DU Cell will be destroyed. It assumes that the sedimentation rates for each glacial cycle are similar. The exact timing of the recurring lakes is not important, the current 100-ky cycle excepted. The Deep Time Model allows the possibility of a deep lake to return in each 100-ky cycle. It also allows intermediate lakes to recur at a frequency that allows the assumed 100-ky sedimentation rate to be satisfied. The current 100-ky cycle is not modeled explicitly. It is possible that the current interglacial period will last for at least another 50 ky due to anthropogenic influences, which is unusually long compared to the interglacial period for recent 100-ky ice age cycles.

5.2 Future Scenarios

Representative lake occurrence scenarios for deep time are described below. Note that there are two components of the models used to represent these scenarios. The first is modeling lake formation and dynamics, based upon the scientific record, literature, and expert opinion. The second is modeling the fate of the Federal DU Cell.

The Great Salt Lake represents the current condition of a shallow lake in the Bonneville Basin. Lakes such as this are likely to exist in all future climatic cycles, but will not reach the elevation of the DU waste embankment at Clive and thus will not affect the waste embankment. For the PA model, it is assumed that destruction of the waste embankment will result from the effects of wave action from an intermediate or deep lake. This assumption separates intermediate and shallow lakes. In this destruction scenario, the embankment material above grade is assumed to disperse through a combination of wave action/churning and dissolution into the water column above the waste dispersal area. Radionuclides present in the embankment dissolve into the lake and eventually return to the lakebed via precipitation or evaporation as the lake regresses.

Some radionuclides in the water column will bind with carbonate ions and precipitate as chemical and biogenic sediment, while radionculides bound to embankment materials will remain within the clastic sediment as the lake eventually recedes. Wave action during the lake recession is expected to rework and mix the chemical, biogenic and clastic lake deposits. The combined complexity of processes affecting the compositional and sedimentary features of lacustrine deposits (Fritz, 1996) and the mixing of lake sediments during regressive and transgressive lake cycles makes it difficult to develop quantitative models of chemical and physical processes affecting the distribution of waste radionuclides in lake waters and sediments.

In reality, waste radionuclides dissolved in lake waters will mix and be diluted by lake circulation driven by prevailing winds and geostrophic balances (Jewel, 2010). Waste-sediment mixes will be dispersed by wave action and longshore drift. Sediment concentrations will decrease over time because the amount of waste does not change other than through decay and ingrowth, whereas more sediment is added over time. The model makes two simplifying assumptions. First, sediments are thoroughly mixed throughout the total sediment depth. In the Deep Time Model the sediment layers are considered to be a single mixing cell. Second, diffusion can occur into the lake through this mixing cell, throughout the total sediment depth. The mixing cell allows for radionuclides to diffuse through a short diffusion length, relative to the depth of the mixing cell (sediment depth). Although sediment concentrations will decrease

over time and lake concentrations would be expected to do so concurrently, lake concentrations do not necessarily decrease over time in the Deep Time Model because of the single mixing cell.

The Deep Time Model assumes that changes in climate will continue to cycle in a similar fashion to the climate cycles that have occurred since the onset of the Pleistocene Epoch. These changes follow those observed in the marine oxygen isotope record (Figure 2). The record captures major climate regime shifts on a global scale and is used in this scenario in conjunction with expert opinion (C.G. Oviatt, personal communication) plus site-specific sediment core and Clive pit wall information to determine the approximate periodicity of lake events. However, uncertainties exist due to the limitations related to the quality of the sediment core data.

It is assumed that during the 100-ky climatic cycles intermediate or deep lakes will reach the elevation of Clive. Although a definitive distinction is not made, lakes that reach the elevation of Clive but do not develop into a deep lake are considered intermediate lakes. These intermediate lakes are also assumed to be large enough that their wave action will destroy the embankment. Intermediate lakes might occur during the transgression and regression of a deep lake, or might occur during a glacial cycle that does not produce a deep lake, perhaps in conjunction with glacial cycles that are shorter and less severe than the 100-ky glacial cycles previously discussed.

In general, variation in lake elevation is assumed to be associated with all types of lakes. The variation is due to local temporal changes in temperature, evaporation and precipitation. For example, the Great Salt Lake has seen elevation changes of several meters in the past 30 to 40 yr. The Great Salt Lake has also seen greater elevation changes in the past 10 ky, but in no cases since the Younger Dryas has the Great Salt Lake reached the elevation of Clive (Oviatt, 2015).

Sedimentation is assumed to occur during these intermediate lake events at higher annual rates than is assumed to occur for the open-water phase of deep lakes. This is based upon the pre-Bonneville lacustrine cycles that are documented in Table 3 (Clive pit wall interpretation, see Appendix A). The lake is assumed to recede after some period of time, at which point a shallow lake (e.g., similar to the Great Salt Lake) will occupy Bonneville basin until the next intermediate or deep lake cycle.

In the deep lake scenario, a deep lake forms throughout the Lake Bonneville basin in response to major glaciation in North America and the Northern Hemisphere, following the ongoing 100-ky glacial cycle. Increases in precipitation and decreases in evaporation over the long term, and subsequent increases in discharge to the Bonneville basin via rivers that drain high mountains along the eastern side of the basin have resulted in lakes that are more than 30 m deep and cover an area similar to that of the most recent deep lake episode (e.g., Lake Bonneville, Provo Shoreline). A similar extent of lake formation (geographic area, lake depth) is assumed to occur in the future. Under such a scenario, the depth of a lake at the location of the Clive facility could be many tens of meters. Resulting lake sedimentation at the Clive site will be high rates of deposition of clastic sediments during intermediate lake events and much slower rates of carbonate deposition during deep lake events. A key difference between the deep lake scenario and the intermediate lake scenario is that both the transgressive and regressive phases of lake formation are considered with the intermediate lake. Transgressive and regressive phases of lake formation can lead to brief periods of rising and falling water levels in both phases. These phases of transgression and regression are also assumed to have higher sedimentation rates than the open-water phase. Upon the complete regression of a deep lake, it is assumed that only intermediate lakes will form until the deep lake associated with the next climate cycle occurs.

6.0 A Heuristic Model for Relating Deep Lakes to Climate Cycles from Ice Core Temperature

6.1 Introduction

In this section, a model is presented for estimating lake elevation that uses surface temperature deviations from the EPICA Dome C ice core data (Jouzel et al., 2007), which is used to support the modeling of future intermediate and deep lakes in the Deep Time Model. The model of lake elevation is not intended to be highly accurate, but rather is aimed at capturing the major lake-cycle features as shown in the studies conducted by Oviatt et al. (1999), Link et al. (1999), and the sediment core and pit wall interpretations (C.G. Oviatt, personal communication). This model is not used as a predictive model but rather to form a basis for the character and dynamics of lake events in the Deep Time Model.

The deep-sea benthic $\delta^{18}O$ record is in excellent agreement with the EPICA Dome C deuterium measurements for the last ~810 ky (Jouzel et al., 2007). Temperature anomaly data for the past 810 ky were obtained from the World Data Center for Paleoclimatology, National Oceanic and Atmospheric Administration/National Climate Data Center. These data are made available based on calculations described in Jouzel et al. (2007), and are plotted in Figure 3. From the 810 ky of data, the temperature deviations range from $T_{min} = -10$ºC to $T_{max} = +5$ºC. This range is used to bound extreme events.

Water balance in the Bonneville basin is affected by many complex processes, so modeling water balance simply as a function of temperature alone is not expected to produce precise results, but instead provides a coarse representation. The conceptual model is based upon a water balance reservoir model of precipitation versus evaporation. If precipitation outpaces evaporation, the lake elevation increases. If evaporation outpaces precipitation, then the lake elevation decreases. Precipitation and evaporation are affected directly by temperature, but long-term patterns of precipitation are affected more greatly by the presence or absence of continental glaciation in North America. Thus, glaciation is modeled first using a simple reservoir model depending on temperature.

6.2 Glaciation

The water balance model begins by constructing a “continental glacier”; an artificial construct that represents a glacier large enough to affect precipitation levels in the Bonneville Basin. The extent of glaciation in proximity to the Bonneville basin is assumed to be zero initially, which is a reasonable approximation for the start time of 785 ka, a start time chosen because it corresponds to a warmer climate phase (data from Jouzel, et al., 2007; see Figure 3). For each time step of 500 yr, an increase in glacial magnitude is dependent on temperature deviation (ΔT) as scaled in Jouzel (see Figure 3):

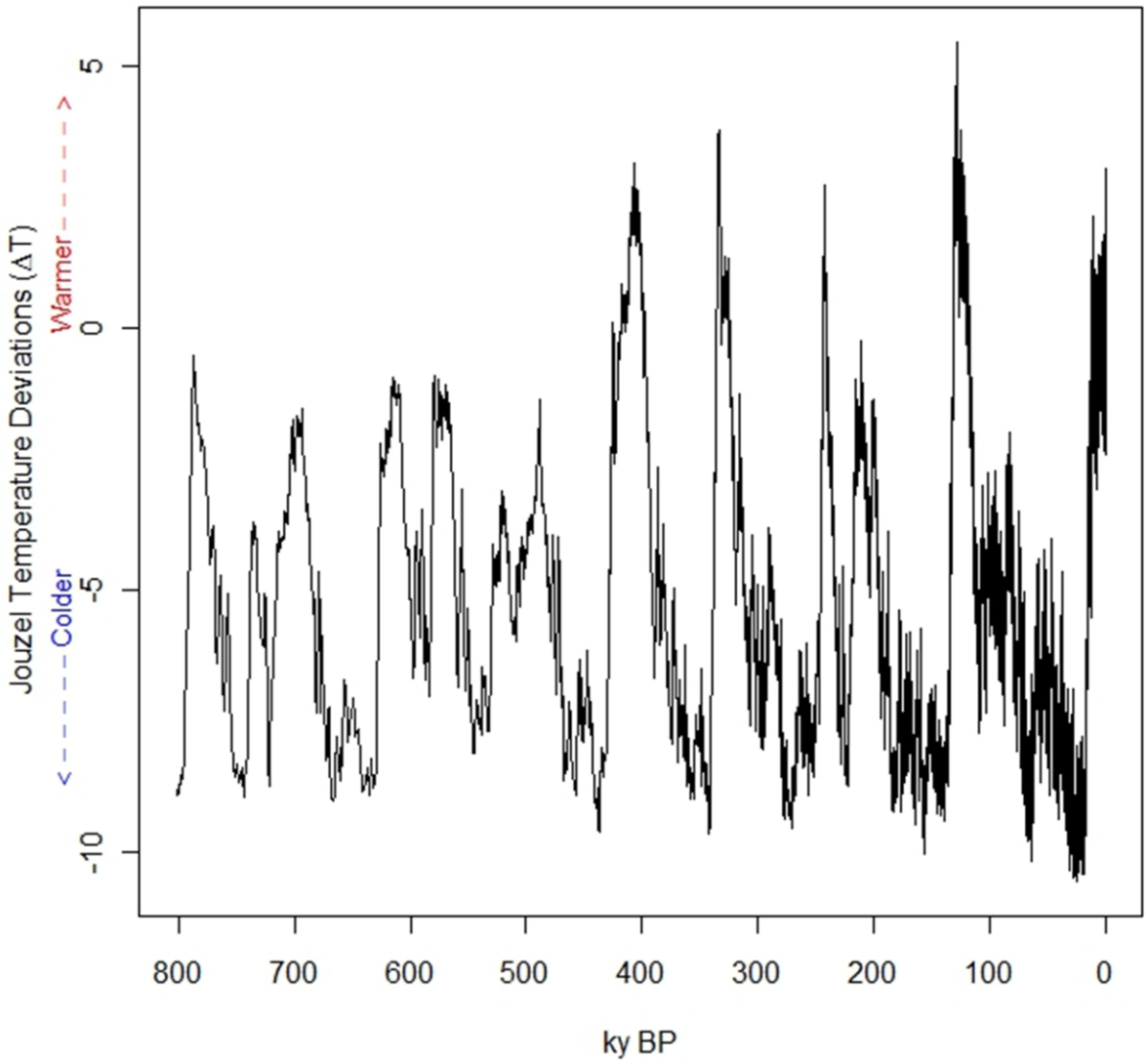

Figure 3. Temperature deviations for the last 810 k (from Jouzel et al., 2007)

$$Glacial_{addition}(\Delta T) = \begin{cases} 0 & \text{if } \Delta T \geq \Delta T_{GMax} \\ \frac{1}{N_{GA}}\left(\left(e^{R_{GA}\cdot(\Delta T_{GMax}-\Delta T)} - 1\right)\right) & \text{if } \Delta T < \Delta T_{GMax} \end{cases} \quad (1)$$

where

N_{GA} is a normalizing constant:

$$N_{GA} = e^{R_{GA}\cdot(\Delta T_{GMax}-\Delta T_{\min})} \quad (2)$$

R_{GA} is a rate parameter (yr^{-1}), and

T_{GMax} is a threshold temperature (degrees Celsius).

As glaciation here is an artificial construct for modeling purposes, the units and scale of the glacial "magnitude" are arbitrary. The parameters of the precipitation model described below must be calibrated appropriately to the scale of the glaciation model.

For each time step, the decrease in glacial magnitude is also modeled as a function of temperature:

$$Glacial_{subtraction}(\Delta T) = \begin{cases} 0 & \text{if } \Delta T \leq \Delta T_{GMin} \\ \frac{S_{GS}}{N_{GS}}\left(e^{R_{GS}\cdot(\Delta T-\Delta T_{GMin})} - 1\right) & \text{if } \Delta T > \Delta T_{GMin} \end{cases} \quad (3)$$

where

N_{GS} is a normalizing constant:

$$N_{GS} = e^{R_{GS}\cdot(\Delta T_{max}-\Delta T_{GMax})} \quad (4)$$

R_{GS} is a rate parameter (yr^{-1}), and

T_{GMin} is a threshold temperature (degrees Celsius).

The change in glacial magnitude for a time step is thus:

$$Glacier_t = max[0, Glacier_{t-1} + Glacial_{addition}(\Delta T_t) - Glacial_{subtraction}(\Delta T_t)] \quad (5)$$

where the *t* subscript is a time step index. The time step used for the model is 500 yr.

The parameters of the model were calibrated heuristically to compute parameters that produced a glacial cycle that appeared reasonable for this coarse model. The set of parameters computed was:

$$\begin{gathered} \Delta T_{GMax} = -6 \\ R_{GA} = 0.25 \\ \Delta T_{GMin} = -6.0 \\ R_{GS} = 0.2 \\ S_{GS} = 5.0 \end{gathered} \quad (6)$$

The change in the glacial magnitude for a particular time step as a function of temperature is shown in Figure 4. These values lead to slow growth during the very cold phases (Jouzel temperature deviations of less than –6°C) of the glacial cycle, and rapid recession during warm phases (temperature deviations of greater than –6°C).

6.3 Precipitation

A coarse model for precipitation in the Bonneville basin was developed dependent on global temperature (as precipitation generally increases with global temperature), lake surface area (which affects recharged evaporation), and an additional effect that depends of the magnitude of the continental glacier. The precipitation in meters of annual rainfall is modeled as:

$$P_t(\Delta T_t, L_{t-1}, G_{t-1}) = B_P + R_{PT} \cdot \Delta T + R_{PLSA} \cdot SA(L_{t-1}) + S_{PG} \cdot e^{R_{PG} \cdot G_{t-1}} \quad (7)$$

where

B_P is a baseline precipitation,

R_{PT} is a coefficient of linear effect of global temperature,

R_{PLSA} is a coefficient of linear effect of the surface area of the lake, and

$SA(L)$ is the surface area in km^2 associated with lake elevation L.

The effect of temperature and lake surface area are modeled as linear, while the glacial effect is exponential with respect to glacier size. The set of parameters calibrated to the glacial magnitude model are:

$$\begin{aligned} B_P &= 0.30 \\ R_{PT} &= 0.005 \\ R_{PLSA} &= 2 \times 10^{-6} \\ S_{PG} &= 0.06 \\ R_{PG} &= 0.03 \end{aligned} \quad (8)$$

The precipitation is then converted to a volume by multiplying by the area of Bonneville basin (approximately 47,500 km^2).

6.4 Evaporation

Evaporation rate in the region is modeled as a function of temperature:

$$E_t(\Delta T_t) = B_E + \frac{S_E}{N_E} \cdot e^{R_E \cdot (\Delta T - \Delta T_{min})} \quad (9)$$

where N_E is a normalizing constant:

$$N_E = e^{R_E \cdot (\Delta T_{max} - \Delta T_{\min})} \quad (10)$$

The evaporation is then converted to a volume by multiplying by the area of the basin.

The calibrated parameters are:

$$\begin{aligned} B_E &= 0.32; \\ S_E &= 0.3 \\ R_E &= 0.05 \\ \Delta T_{min} &= -10 \\ \Delta T_{max} &= 5 \end{aligned} \tag{11}$$

If the precipitation volume exceeds the evaporation volume, then the difference is added to the lake volume, and the lake elevation is calculated from the total lake volume.

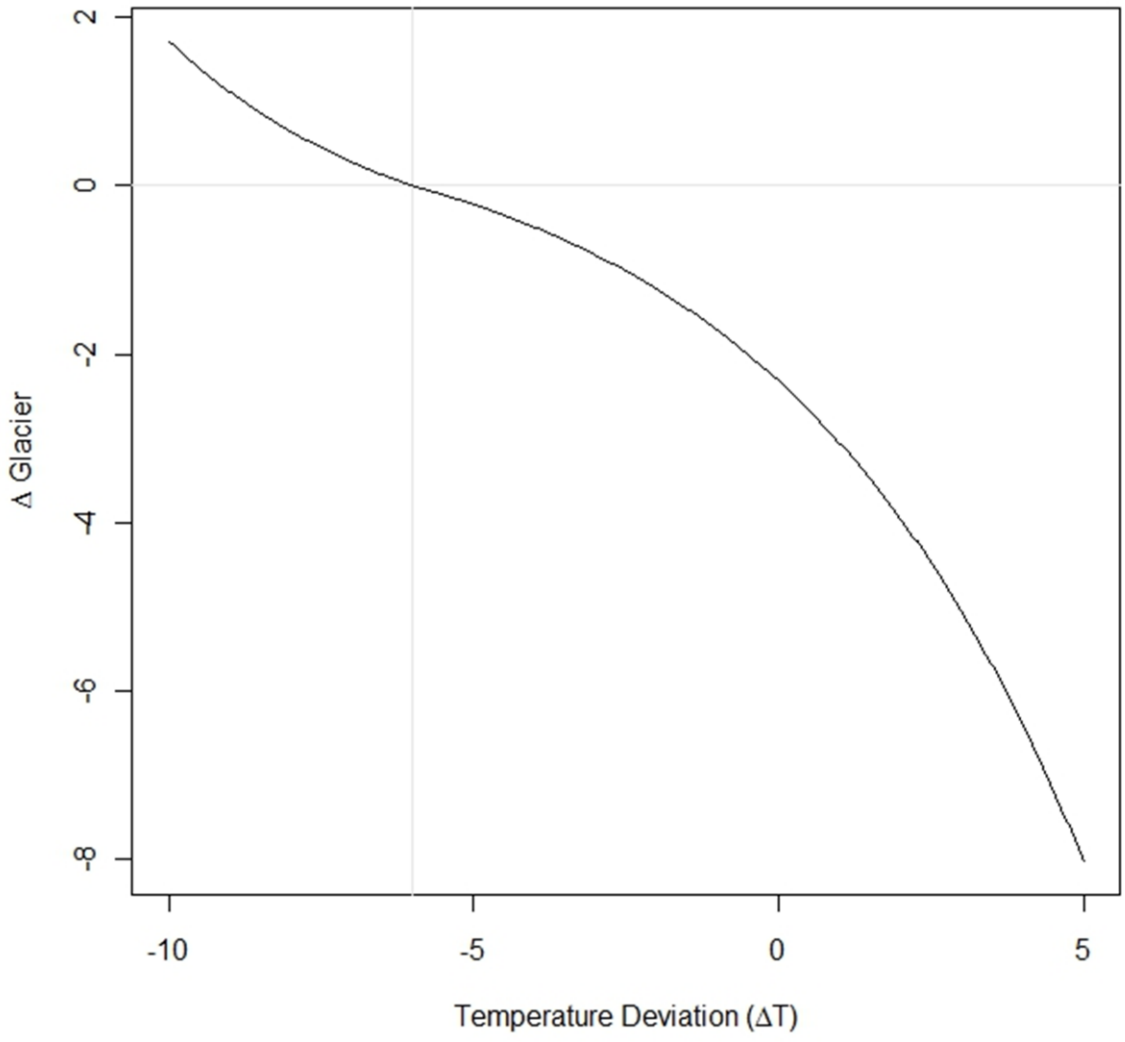

Figure 4. Glacial change as a function of temperature for the coarse conceptual model

If the evaporation volume is greater than the precipitation volume, then the total evaporation is adjusted downward to adjust for the actual surface area exposed (rather than the full surface area of the basin as used in the initial calculation). The difference between the adjusted evaporation and the precipitation is then subtracted from the lake volume, and the lake surface elevation is calculated from the total lake volume.

$$\Delta Volume_t = \begin{cases} [P_t(\Delta T_t) - E_t(\Delta T_t)] \cdot SA_{basin} & \text{if } E_t(\Delta T_t) < P_t(\Delta T_t) \\ [P_t(\Delta T_t) - E_t(\Delta T_t)] \cdot \dfrac{SA(L_{t-1})}{SA_{basin}} & \text{if } E_t(\Delta T_t) \geq P_t(\Delta T_t) \end{cases} \quad (12)$$

6.5 Simulations

For simplicity, lake volume and glacial magnitude are assumed to be zero at the first time step (785 ka), as that time step corresponds to a warm climate phase. The values for the parameters given above are calibrated graphically to produce reasonable precipitation versus evaporation values. Several lake elevation histories were simulated by simulating the parameter values of the model probabilistically. The distributions for the parameters were lognormal with medians equal to the parameter values listed in Equations (6), (8), and (11). The simulations provide a variety of behaviors depending on the combination of parameters simulated.

A few common features are apparent in the simulated results. The largest lakes tend to occur at the times of Lake Bonneville, Little Valley, and Lava Creek, and the smallest 100-ky cycle lake occurs in δO^{18} cycle 14 (~533 ka), which matches the scientific record. When the simulated glaciation effects are small (R_{GA} and R_{GS}), precipitation change in the model is due primarily to temperature change. In this case, deep lakes form with few intermediate lakes, as the lake elevation history in the top graph in Figure 5 shows. When glaciation effects are larger, then deep lakes tend to last longer, and intermediate lakes form, as the lake elevation history in the lower graph of Figure 5 shows.

The simulation models were then calibrated further by combining the simulated lake histories with sedimentation rates seen in sediment cores. Based upon the results of this coarse model calibration, some assumptions are carried forward to the Deep Time Model.

1. The 100-ky cycle in global temperature is a strong indicator of the return of a deep lake. While not all simulations showed a lake returning to the Clive elevation in every 100-ky cycle (particularly δO^{18} cycle 14), the results were consistent enough to treat as systematic behavior for a heuristic model.

2. Intermediate lakes should be a part of the Deep Time Model, because sedimentation rates did not calibrate well with simulations that produce only deep lakes.

3. Intermediate lakes are more likely to occur in the later stages of the 100-ky cycle than in the early stages, primarily in conjunction with the slowly decreasing temperatures across the cycle (as opposed to the relatively rapid warming period that occurs at the end of a 100-ky cycle).

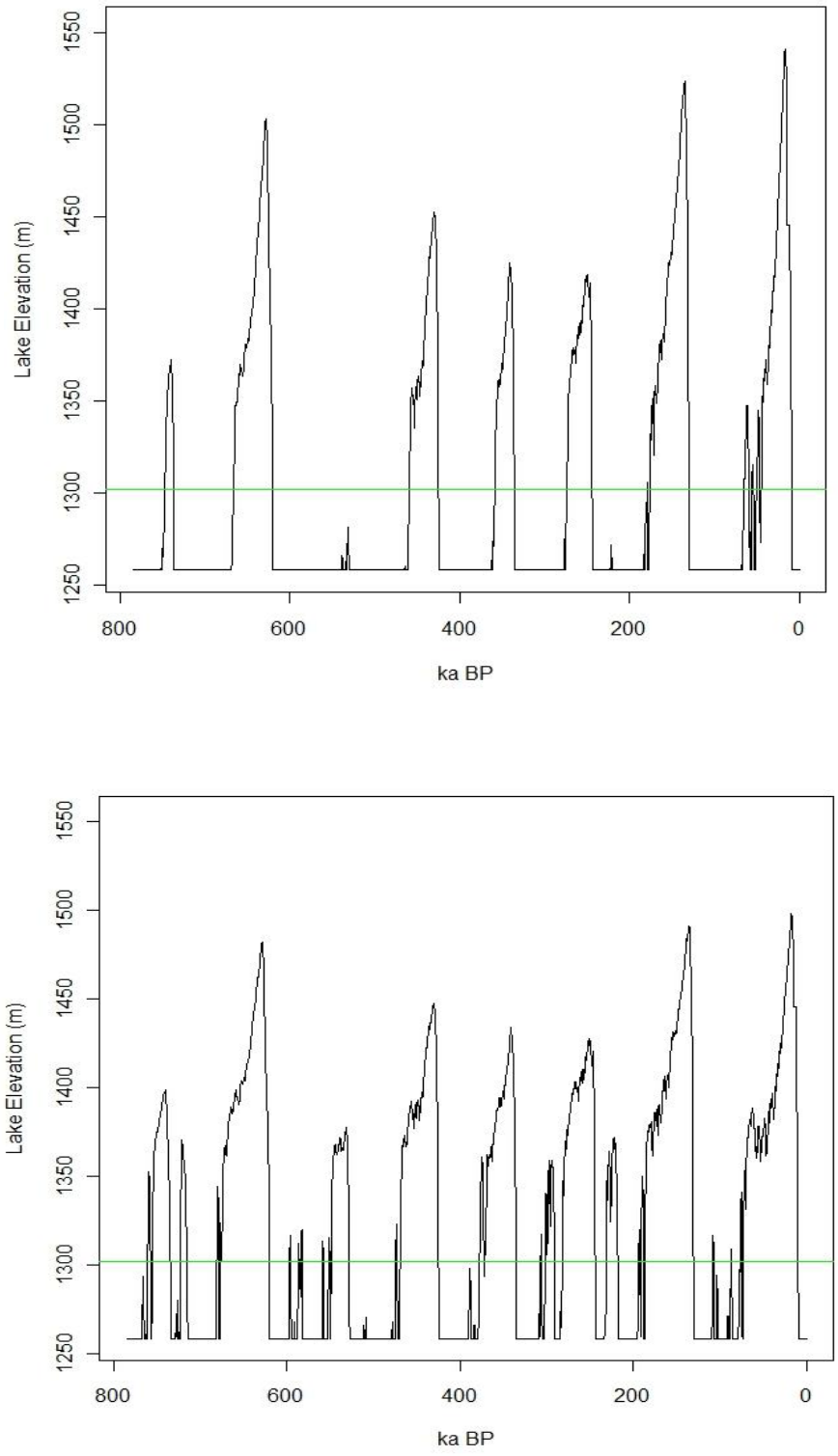

Figure 5. Two example simulated lake elevations as a function of time, with Clive facility elevation represented by green line

7.0 Deep Time Modeling Approach

7.1 Introduction

The GoldSim systems analysis software (GTG, 2011) is used to construct the Clive DU PA Model v1.4. The same Species list of contaminants, material properties, and site geometry are retained from the Clive DU PA Model v1.2. The standalone DTSA Model is combined with the deep time container of the Clive DU PA Model v1.2 in the Clive DU PA Model v1.4 deep time container.

The DU waste inventory for the start of deep time is taken from the Clive DU PA Model v1.4 Federal DU Cell Disposal container at the time the first lake returns, which changes for each realization. The DU waste is disposed below current grade. Contaminant fate and transport are captured in the Federal DU Cell until the first lake returns. Radionuclides above grade when the first lake returns are dispersed across the lake area and assumed to be available to diffuse into any lake that appears. "Above ground" radionuclides are assumed to be at least 2 m above the original ground surface, where eolian processes deposit at least 2 m of material in the 50,000 years or more before a lake returns. Remaining radioactivity in the lowest six waste layers (about the lowest 2.5 m of the embankment) at the time the first lake appears is used as the Rn flux inventory for the Deep Time Model.

The Deep Time Model is largely a heuristic representation of deep time. The underlying concepts are that a lake will return to the elevation of Clive at some point in the future, and new lake sediments will be sufficiently thick after the first lake recedes that radon flux will meet regulatory guidelines. Contaminant fate and transport after the first lake returns are not evaluated in the Deep Time Model, excepting radioactive decay and the ingrowth of progeny.

As previously discussed, the depth of lake and eolian sediments removed at the Clive location due to wave action and the residual material from the destroyed embankment are expected to be approximately equal, and their effects essentially cancel. Therefore, the thickness of residual embankment material and sediment overlying the disposed DU waste at the time when the first intermediate lake recedes will be effectively equivalent to the thickness of eolian sediments deposited up until that point in time, represented by the rising elevation of the surrounding grade. The Deep Time Model calculates radon ground surface flux from radionuclides in the disposed DU waste buried beneath this layer. Dose to a rancher from this radon flux is calculation to provide a reference point to interpret the significance of the radon flux.

7.2 Deep Lake Characteristics

The 100-ky climate cycle is treated as a sufficiently robust effect to create a hypothetical lake that will reach and exceed the elevation of the Clive site during each glacial cycle. The exact time of occurrence is not a crucial parameter, due to the slowly-changing concentrations during deep time. Thus, the lake is set to be present during each 100-ky interval, with time beginning at 10 ky (the end of the performance period for the quantitative dose assessment component of the PA).

There is limited information from the Quaternary geologic record for the duration of time that the Clive location has been under water. Lake Bonneville has been estimated to have been present at the elevation of Clive for an interval of approximately 16 ky (Oviatt et al., 1999). Durations of pre-Lake Bonneville deep lakes are uncertain. Thus, a conservative choice was made to allow deep lakes to remain an average of about 20 ky (conservative in the sense that more radionuclides will migrate into the water column). The occurrence time for each deep lake is set by choosing a start time some number of yr prior to the 100-ky mark. The start time is represented by a lognormal distribution with geometric mean of 14 ky prior to the 100-ky mark, and a geometric standard deviation of 1.2. The end time is represented by a lognormal distribution with geometric mean of 6 ky after the 100-ky mark, and a geometric standard deviation of 1.2. These distributions are depicted in Figure 6.

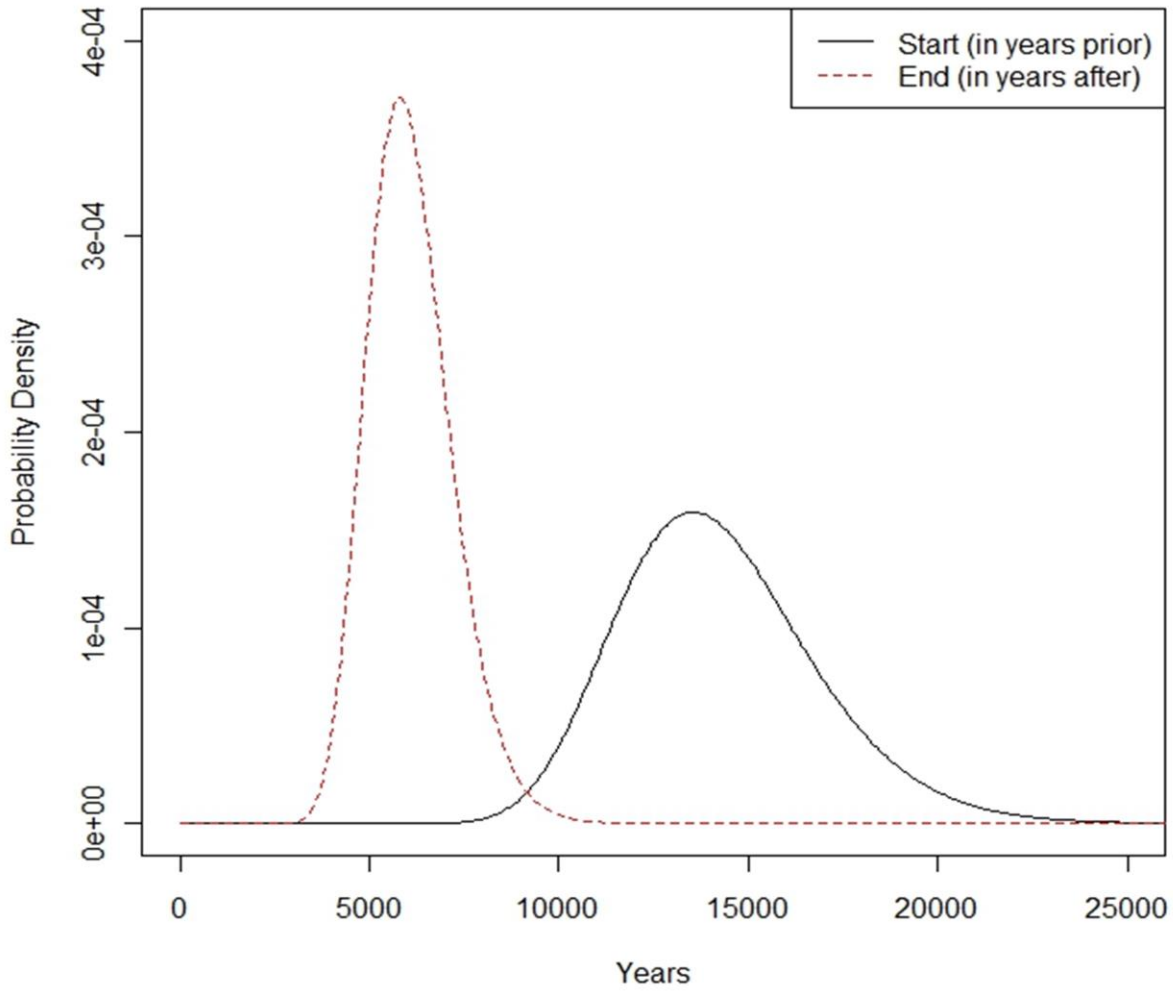

Figure 6. Probability density functions for the start and end times for a deep lake, in yr prior to the 100-ky mark and yr after the 100-ky mark, respectively.

7.3 Intermediate Lake Characteristics

Intermediate lakes are modeled as potentially occurring during the transgressive and regressive phases of deep lakes and at any time between deep lake events. In order to reflect the slow decrease in temperature over the 100-ky cycle, the occurrence time for intermediate lakes is modeled as a Poisson process with a rate that increases linearly over the cycle time, from a rate of 0 to 7.5 lakes per 100 ky. This process produces an average of about 3 intermediate lakes per 100 ky. There is little recorded basis for this number, but it matches reasonably with the heuristic model and was chosen so that long-term sedimentation rates matched the average clastic sediment thickness observed in studies of lake cores from previous lake cycles.

There is virtually no information for the duration of intermediate lakes, due to the high mixing rate of lake sediments, which prohibits establishing the chronology of individual stratigraphic layers from studies of cores of intermediate lake sediments. Thus, a distribution was chosen to roughly calibrate with the heuristic model: lognormal with geometric mean of 500 y and geometric standard deviation of 1.5.

7.4 Sedimentation Rates

As previously mentioned, the Deep Time Model makes a distinction between deep and intermediate lakes with regard to sedimentation.

- The sedimentation patterns of deep lakes are assumed to be similar to observed intervals of carbonate marl from Lake Bonneville or Lake Provo, and are assumed to occur no more than once per 100-ky glacial cycle. The depth of deep lakes is significantly greater than the depth of wave action and slow precipitation of carbonate is assumed to be the dominant sedimentation process.
- Intermediate lakes are defined as lakes that reach and exceed the altitude of the Clive site but are not large (or deep) enough that carbonate sedimentation is the dominant mode of lake sedimentation. The transgressive and regressive phases of the Bonneville and Provo shoreline lakes represent intermediate lakes formed during transient lake cycles where the lake levels exceeded the elevation of Clive and lake sedimentation was dominated by clastic deposits associated with wave activity and reworking of pre-existing lake and eolian sediments (see Table 2 for the chronology of the lake cycles).
- Shallow lakes, similar to the modern Great Salt Lake, are assumed to exist at all other times, but these are irrelevant to the geomorphology of the Clive site and thus are not explicitly modeled.

Deposition of eolian and lake sediments in the area of the Clive facility is a continuous process that occurs during shallow, intermediate and deep lake periods. During shallow lake periods, as observed in present-day conditions, eolian deposition of sand, and silt/loess is the primary sedimentary mechanism. However, eolian deposits are rarely observed in sediment cores, presumably because of reworking of the depositions during lake transgressions and mixing with lake-derived sediments. Note however that the upper part of the Clive quarry exposure is now known to be of eolian origin (Neptune, 2015a) and paleosoils and eolian deposits have been observed in the pre-Lake Bonneville sedimentary deposits at Clive and described in the Burmester core indicating prolonged periods of subaerial exposure. Intermediate lake sediments

include chemical, biogenic, and terrigenous sediments, with their proportions dependent on the size and duration of the lake and the interplay between deep lake deposition and near-shore sedimentary processes. Schofield et al. (2004) note that the large fetch of Lake Bonneville (distance of wave forming winds over the water) produced a variety of wave-dominated erosional and depositional sedimentary and geomorphic features. They identified cross-sections of erosion-dominated and deposition-dominated shorelines and the composite sedimentation rates of shoreline profiles will be dependent on local process of wind/wave erosion and deposition and supply of sediments from alluvial fans flanking pluvial lakes (Schofield et al., 2004). Moreover, eolian depositional layers are not commonly observed in the sediment cores, so the model effectively combines eolian deposits with lake sediments. The mixing probably occurs during intermediate lake cycles, which are likely to be the first lakes after interglacial periods. These assumptions require that there is a mixing depth associated with each lake recurrence. However, the mixing process itself makes it difficult to assign mixing depths for the different layers in the sediment cores. Mixing depths are probably determined by the dynamics of wave activity and resulting erosion/deposition during lake transgressions and regressions.

Deep lakes, in contrast, have similar sediment deposition rates to intermediate lakes in their transgressive and regressive phases, but have slower rates of sedimentation when the lake is deep enough that the dominant process is predominantly precipitation of chemical and biogenic material from the lake waters. Studies of the sediment cores are able to distinguish between layers associated with intermediate lakes with predominant sediment mixing, and sedimentary layers associated with a deep lake that are dominated by carbonate layers (marl).

For deep lakes, a sedimentation rate is modeled as a lognormal distribution with geometric mean of 120 mm/ky and geometric standard deviation of 1.2, a distribution that covers the range of observed values for deep lakes. This distribution is represented in Figure 7. The sedimentation rate is applied for the simulated duration of the deep lake. In addition, sedimentation is added at the beginning of the lake cycle as well as the end that represents the shallow phase of the transgressive and regressive lakes. This additional sediment mimics the behavior of an intermediate lake.

For intermediate lakes (and shallow phases of deep lakes), there is high likelihood of multiple short-term transgressions and regressions with respect to the elevation of Clive. For example, the Clive pit wall (Appendix A) shows three distinct lakes after the deep-water phase of Lake Bonneville and three distinct lakes prior to the deep-water phase of Lake Bonneville. Without further systematic study of sediment cores and trench sections in and around the Clive site, including chronology studies, it is impossible to determine if these distinct lakes were separated by a few years or a few hundred years; i.e., whether they are distinct lake events or simply part of the transgression and regression of Lake Bonneville. However, based upon current behavior of the lake, some year-to-year variation in the lake elevation occurs, in addition to the longer-term trends in lake elevation.

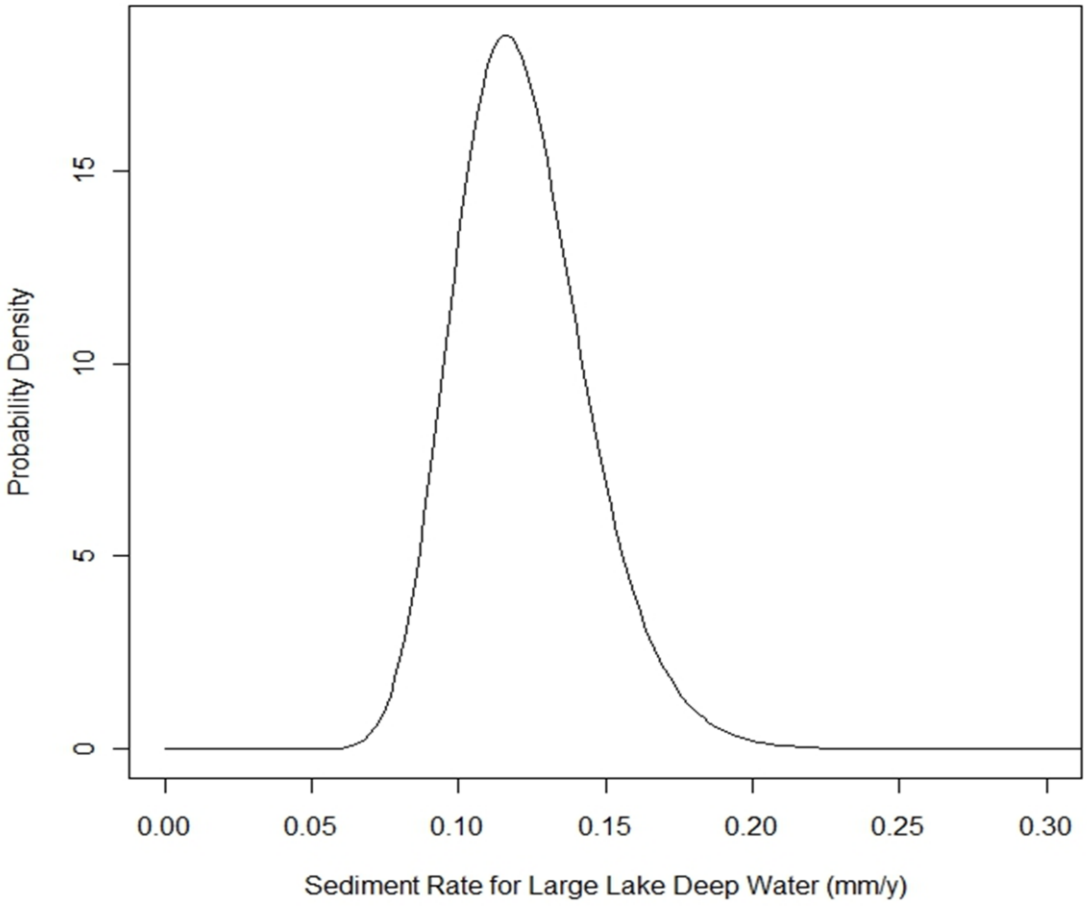

Figure 7. Probability density function for sedimentation rate for the deep-water phase of a deep lake

Another heuristic model was constructed to evaluate the effect of the short-term variation. The lake elevation for the years 1848 through 2009 is available from the Saltair Boat Harbor monitoring site (USGS, 2001), as shown in Figure 8. The year-to-year variation can be modeled as a second-order autoregressive process AR(2) (Brockwell and Davis, 1991), a model that accounts for year-to-year temporal correlations in the variation. An AR(2) process was simulated and added to a transgressive or regressive curve based upon the simplified model previously presented. Examples of these simulations are given in Figure 9. As can be seen in the figure, the short-term variation can result in lakes covering the Clive elevation for a short time, receding for a short time, then rising again, often multiple times in a single transgression cycle. A similar simulation was performed for simulated intermediate duration lakes as well. The transgressive and regressive phases of a deep lake are assumed to behave similarly to the intermediate lakes in that they averaged about four total occurrences of "mini-lakes;" i.e., occurrences of a rise above the elevation of Clive followed by a drop below for at least one year.

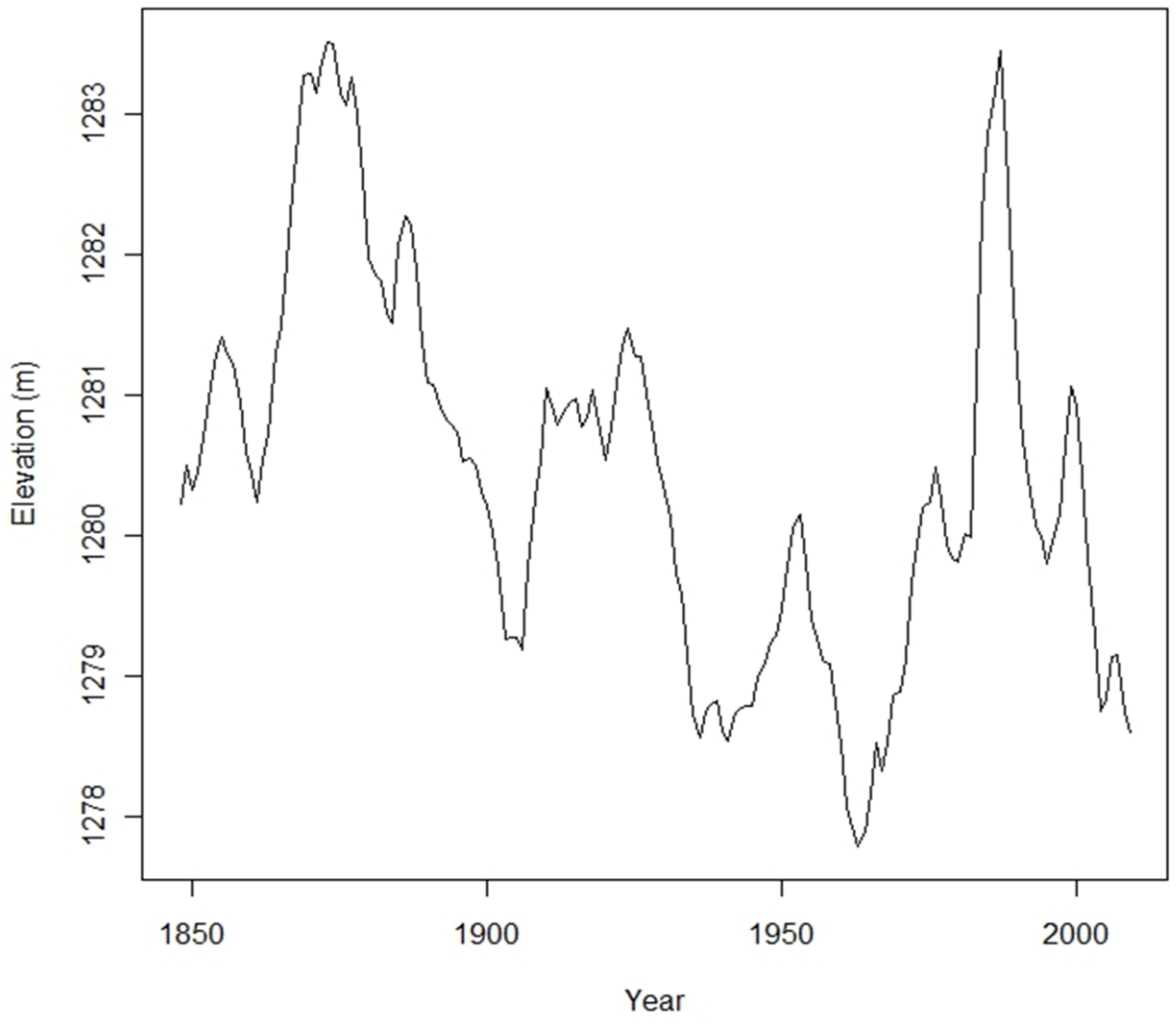

Figure 8. Historical elevations of the Great Salt Lake

The distribution for sediment thickness for intermediate lakes was thus based upon simulating this multiple mini-lake behavior. First, the number of mini-lakes associated with an intermediate lake was simulated as 1 plus a Poisson random variable with rate 3 (the "plus 1" being necessary to ensure at least one event in order to match the definition of a lake event). The sedimentation for each mini-lake was simulated using a distribution based upon the sedimentary deposits of mini-lakes exposed in the Clive pit wall, using the six distinct "mini-lakes" in Table 3 (all layers except the one that corresponds to the deep-water phase of Lake Bonneville). These data are represented in a lognormal distribution of sediment thickness with geometric mean 0.75 m and geometric standard deviation 1.4.

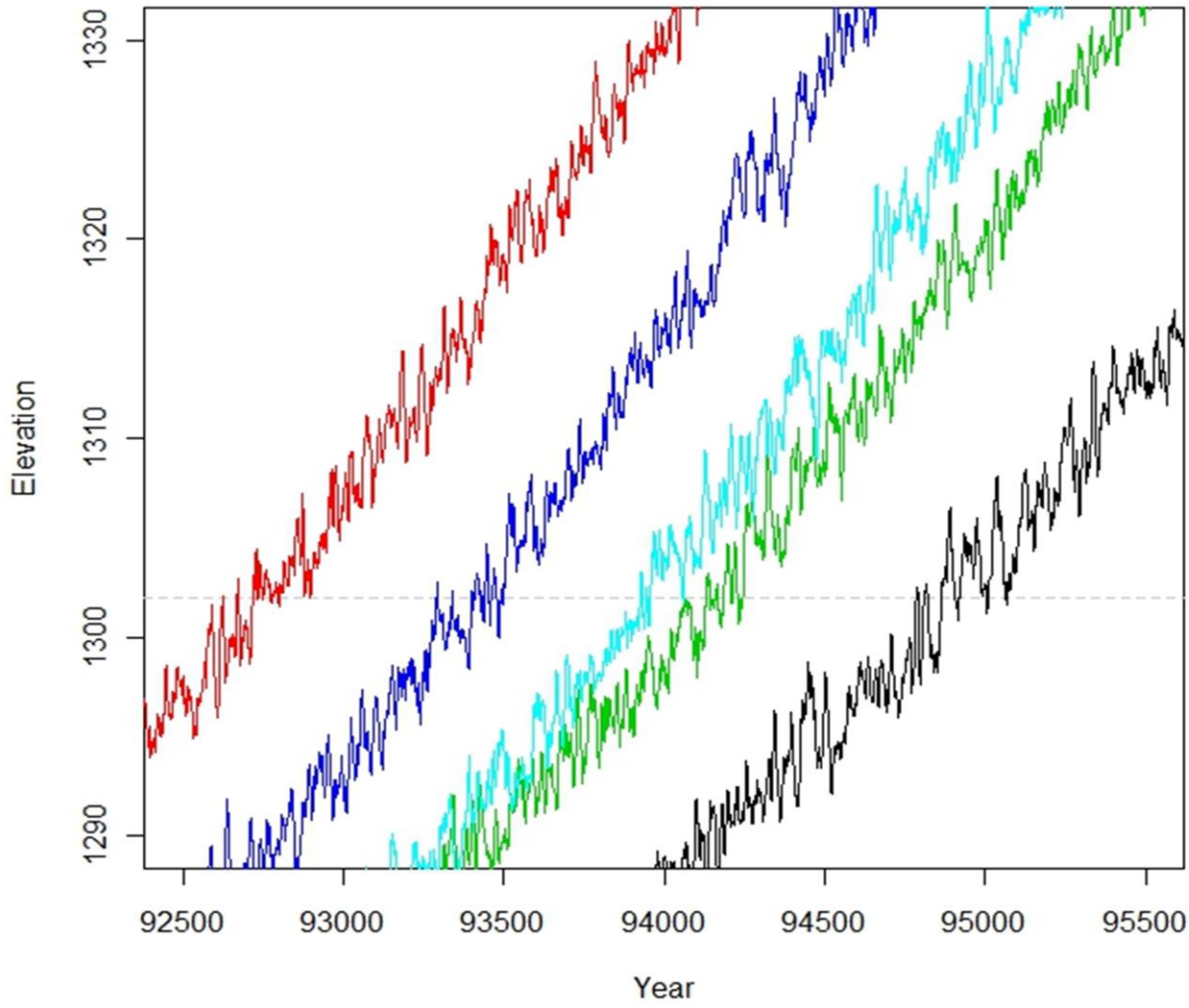

Figure 9. Simulated transgressions of a deep lake including short-term variations in lake elevations

The total sedimentation for all mini-lakes associated with a simulated intermediate lake cycle was then added together to produce a total sedimentation for the intermediate lake. A distribution was then based upon all simulated intermediate lake sedimentations, a lognormal distribution with geometric mean 2.82 m and geometric standard deviation 1.71, as presented in Figure 10. Note that the sedimentation pattern for intermediate lakes is represented as a distribution of composite sediment thickness and contrasts with a distribution of sedimentation rates assumed for deep lakes. The net effect is that the sedimentation rates are on the order of 15 to 20 m per glacial cycle (100-ky). For the duration of the model (2.1 My), this implies sedimentation of more than 300 m. The Basin and Range system accommodates this rate of sedimentation because it is an extensional system; i.e., sedimentation continues as the basins expand and subside, maintaining similar elevation in each cycle.

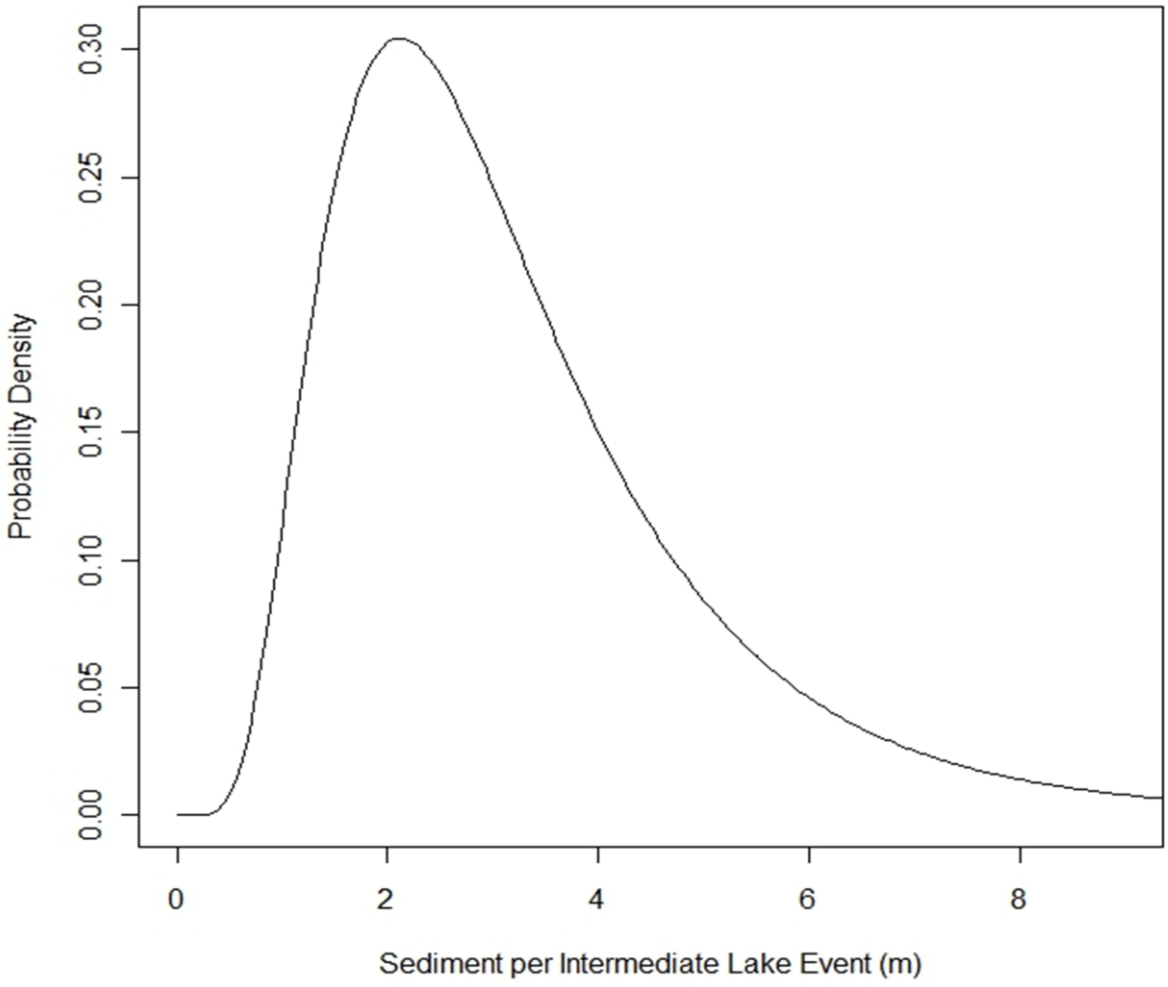

Figure 10. Probability density function for the total sediment thickness associated with an intermediate lake (or the transgressive of regressive phase of a deep lake)

7.5 Eolian Depositional Parameters

Studies of eolian deposits in multiple quarry exposures at the Clive site and in surface exposures west and southwest of the site show that deposition of eolian sand and silt is now occurring and will continue to occur in the future as long as the at grade site elevation is exposed at the surface (above the elevation of lake levels; Neptune, 2015a).

7.5.1 Field Studies

Field studies of the eolian depositional history at the Clive Disposal Site were conducted in December 2014 to provide information for characterizing eolian deposits and establishing eolian depositional rates for the original DTSA Model (Neptune, 2015a). The primary goals of the field

studies were to evaluate the modern geological and depositional setting of the Clive site, and to assess the stratigraphy of the Holocene and Pleistocene lake sedimentation of Lake Bonneville and post-lake depositional processes within the Clive site including the following:

1. Re-evaluating the stratigraphic section previously described by Oviatt (1985, cited in Neptune, 2015b).
2. Describing the eolian sediments and processes affecting the sediments.
3. Measuring variations in thickness of the deposits across the site.
4. Providing sufficient replicate measurement at multiple sites to estimate eolian sediment thicknesses and the variation in eolian sediment thicknesses at the Clive site.

The field studies achieved these primary goals, and the replicate measurements of the thickness of eolian deposits located in the upper part of the stratigraphic section were made at multiple locations on and in the vicinity of the Clive Disposal Site. The data are presented in Neptune (2015) and are used below to develop input probability distributions for the Deep Time Model.

7.5.2 Probability Distributions for the Depth and Age of Eolian Deposition

The Deep Time Model requires specification of input probability distributions for the depth of eolian deposition and the age of the eolian deposits. Together, these two variables provide the information needed to estimate the rate of eolian deposition. The distribution for the depth of eolian deposition is based on the field data described above (Neptune, 2015a), whereas the distribution for the age of the eolian deposits are derived from a summary paper by Oviatt (2015).

An assumption is made that the described eolian deposits at the Clive site represent an integrated time interval of eolian sediment accumulation, modification by processes of soil formation and minor modifications by processes of surface erosion. These deposits approximate a steady-state representation of eolian processes since the regression of Lake Bonneville and these processes should continue into the future until conditions at the site change considerably (e.g., natural climate change). The distributions are based on the depth of eolian deposition since Lake Bonneville regressed below the elevation of Clive and estimations of the age at which regression below the Clive elevation occurred (Neptune, 2015a) These distributions are used to model future eolian deposition until the return of a lake at the elevation of Clive.

The data presented in Table 4 from Neptune (2015a) are the measured thicknesses of eolian silt in quarry walls and excavated surfaces for the Clive Disposal Site. The mean of the deposits is 72.7 cm, and the standard deviation is 16.6 cm. There are 11 data points, and the data are reasonably symmetric about the mean. Consequently, a normal distribution is specified for the Deep Time Model with a mean of 72.7 cm and a standard error of 5.0 cm. A reasonable simulation range considering ± 3 standard errors would be 57.5 to 87.5 cm. The minimum of the normal distribution was set to a very small number and the maximum was set to a very large number so that the distribution was not unnecessarily restricted.

This distribution represents spatio-temporal scaling, so that the distribution is of the average depth of eolian deposition at the Clive site since Lake Bonneville regressed below the site. This provides the best representation of the future eolian depositional rates over the long timeframes and spatial scales of the Deep Time Model.

Table 4. Thickness measurements from field studies of eolian silt near Clive

Neptune Field Studies December 2014				
Site	**GPS Coord** UTM E	**GPS Coord** UTM N	**Silt Thick** (cm)	**Date** (mm/dd/yy)
Clive 29-1	321354	4508262	90.0	12/16/14
Clive 29-2	321390	4508256	80.0	12/16/14
Clive 29-3	321423	4508248	80.0	12/16/14
Clive 29-4	321502	4508236	60.0	12/16/14
Clive 29-5	321239	4508283	110.0	12/16/14
Clive 5-1	320813	4504729	55.0	12/16/14
Clive 5-2	320869	4504730	70.0	12/16/14
Clive 5-3	320914	4504731	60.0	12/16/14
Clive 5-4	321041	4504732	70.0	12/16/14
Clive Hand-Dug-1	322093	4507482	70.0	12/17/14
Clilve hand-Dug-2	320445	4507035	55.0	12/17/14
		Mean	**72.7**	
		Std Error	**5.0**	

Note that several replicate measurements were taken at each location (usually three or four), and the results represent the average thickness at each location. These data are also supported by previous data collected from shallow core studies at Clive, which also are presented in Neptune (2015a). The documentation and uncertainty in the measurements of the eolian sediment thickness from the core studies data is not as precise as those made in the Neptune field study; however, the data are supportive of the results of the field study, indicating very similar patterns of eolian thickness data. These data provide another 21 data points that have an average of 71 cm depth of eolian deposits, with a standard error of 4 cm. Because of the uncertain pedigree and lesser precision of the data from the core studies, they were not used in the distribution development. Their use would have resulted in a much tighter distribution because of the scaling effects of spatio-temporal averaging.

Ages of the deposits were determined from radiocarbon dating. The summary paper by Oviatt (2015) provides the most recent compilation and interpretation of radiocarbon ages for the chronology of Lake Bonneville. Based on information summarized in Figure 2 of Oviatt (2015) and supported by the supplemental radiocarbon data referenced in the paper, the preferred estimate for the age of the final regression of Lake Bonneville below the altitude of the Clive site is about 13.5 ka. (Clive elevation 1304 m). A reasonable lower bound on the youngest or minimum age for this event is 13.3 ka based on radiocarbon ages determined from organic material collected in post-Bonneville wetland deposits (Oviatt, 2015). The reasonable oldest or maximum age of lake regression at the Clive site is constrained by the age of the Provo shoreline and reliable radiocarbon ages for sites above the altitude of the Clive site and below the Provo shoreline. This reasonable maximum age is estimated to be about 14.5 ka. A distribution was developed based on these values from Oviatt (2015) and on expert elicitation of Oviatt. Oviatt suggested that values around 13.5 ka were more likely. Based on this information a beta distribution was fit to approximate elicited quantiles. The following quantile inputs were used:

- Absolute minimum possible age – 13,000 yr
- Reasonable minimum age – 13,300 yr
- Most likely age – 13,500 yr
- Reasonable maximum age – 14,500 yr
- Absolute maximum possible age – 15,000 yr

After considering possible quantiles for the middle three terms, a beta distribution fit was agreed upon with the following parameters:

- Minimum – 13,000 yr
- Maximum – 15,000 yr
- α (shape 1 parameter) – 3.318
- β (shape 2 parameter) – 7.498

This beta distribution has a mean of approximately 13,600 yr and a standard deviation of approximately 270 yr. The mean is reasonably close to the specified most likely age of 13,500 yr. Quantiles of this beta distribution are provided below:

- 2.5% – 13,174 yr
- 10% – 13,284 yr
- 20% – 13,378 yr
- 50% –13,592 yr
- 80% – 13,846 yr
- 90% – 13,988 yr
- 97.5% – 14,207 yr

The distribution is slightly positively skewed, hence the median is slightly less than the mean, and the difference between the maximum and the median is greater than the difference between the minimum and the median. Note that averaging is not employed for this distribution. The distribution simply reflects the age over which eolian deposition has occurred. The rate of eolian deposition is averaged for spatio-temporal scaling by dividing the depth of deposition by the age over which deposition has occurred as described in the next section.

In principle, the rate of eolian deposition is the deposition thickness divided by the age over which deposition occurs. However, an assumption is made that greater ages imply greater depths, in which case there is a correlation between depth and age of eolian deposition. There are no data to inform a correlation between these two variables. Although elicitation could be performed to develop a correlation, the approach taken is to specify the correlation as uncertain across a range of 0.5 to 1. In a sense, this distribution is chosen to indicate that the "data are more likely to be correlated than not-correlated." A uniform distribution is used across this range, but this input will be tracked specifically in sensitivity analysis to determine if it is an important predictor of the Deep Time Model output.

Using the input distributions and the correlation described above, the resulting distribution of rate of eolian deposition in the model has a mean of approximately 5.3×10^{-5} m/yr, (roughly 53 cm every 10 ky) with a standard deviation of approximately 3.0×10^{-6} m/yr. A histogram of the eolian deposition rate for 1,000 realizations is depicted in Figure 11. Quantiles from these simulated data include:

- 5% – 4.84E-05 m/yr
- 10% – 4.96E-05 m/yr
- 20% – 5.10E-05 m/yr
- 50% – 5.34E-05 m/yr
- 80% – 5.58E-05 m/yr
- 90% – 5.71E-05 m/yr
- 95% – 5.81E-05 m/yr

The distribution is symmetric, as evidenced by the normal distribution fit that is laid over the histogram. The normal distribution has the mean and standard deviation as specified above, and the quantiles, which show similar differences between the 95% quantile and the median and the 5^{th} quantile and the median.

Overall, this intermediate product of the Deep Time Model suggests eolian deposition rates of slightly more than 0.5 m every 10,000 yr.

7.6 Destruction of the Federal DU Cell

Destruction of the Federal DU Cell embankment was modeled assuming future lakes have sufficient wave energy to destroy the above-ground portions of the cell. The precise lake elevation needed for this to happen is not considered for the model, but the intermediate lakes that occur in the model are intended to match this definition.

The first lake in the time period assessed is more likely to be an intermediate lake but can be either an intermediate or a deep lake. The destructive energy is equivalent in either case, as the conceptual model treats the transgressive phase of a deep lake as behaving similarly to an intermediate lake.

The mass of material that is within the embankment above the grade of the surrounding land is assumed to be eroded to grade and dispersed by wave action. This volume of above grade material in the embankment, including fill material and cap material, is assumed to be mixed with the sediment associated with the intermediate lake, and subsequently spread across a dispersal area determined by the dynamics of wave activity.

The dispersal area parameter used in the original Deep Time model was estimated for a projected area where the above grade embankment material could be spread by wave action using different assumptions for the final dispersal thickness of the volume of embankment material. The dispersal area was designed to be conservative (small sediment dispersal areas) giving higher waste concentrations in sediment allowing increased dissolution of waste in lake water.

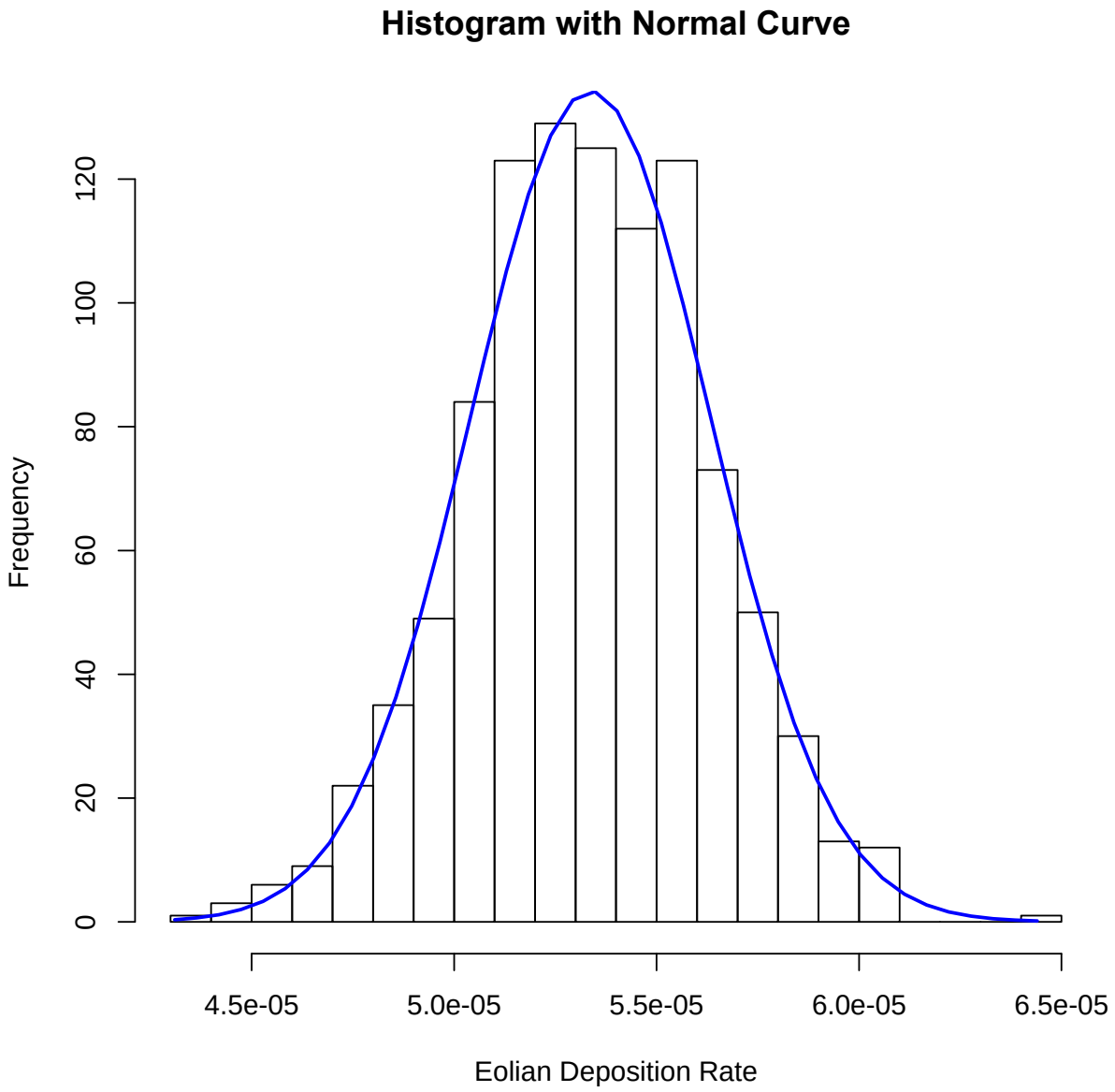

Figure 11. Eolian deposition rate results for 1,000 realizations (m/yr).

With below grade disposal of DU, the approach to estimating the dispersal area is revised and based on a conceptual model for processes affecting the Clive disposal site with the return of a lake. The following assumptions are used for the revised lake return scenario:

1. The Clive site will be affected by the return of a lake at some time in the future. The lake event will be either an intermediate lake or the transgressive phase of a deep lake with the lake processes the same for either event (degradation of the site by near-shoreline wave action).

2. Eolian deposition will occur during the interval after waste emplacement and before the first return of a lake to the elevation of the Clive site.
3. Wave action associated with the lake return is assumed to completely remove the above-grade embankment material above the DU waste.
4. Wave action will churn (rework) the eolian deposits and lake sediments. The maximum depth of reworking of the eolian deposits is assumed to be about 1 meter based on the geometry of shoreline deposits for Lake Bonneville.
5. Radionuclides within the above grade embankment will be dispersed by wave action and mixed with eolian deposits and lake sediments.
6. The alternative models used for estimating sediment dispersal areas include:
    a. Analogue sites of modern sedimentary processes dispersing sediments at shorelines of the Great Salt Lake;
    b. Field assessments of sediment dispersal during the transgressive phase of Lake Bonneville at and around the Clive Disposal Area (Neptune, 2015a);
    c. Assessment of wind directions from dune forms west and southwest of Clive (Jewell and Nicoll, 2011)

Google Earth© imagery was used to identify and determine the areas of active shoreline sedimentation for the Great Salt Lake assuming these patterns provide analogues for wave action and sediment dispersal for the lake return scenario at Clive. Dispersal area estimations assumed no longshore drift (minimum areas) and one dominant direction of longshore drift (maximum areas). The Great Salt Lake analogue may be somewhat conservative (underestimate sediment dispersal) for two reasons. First, the fetch length for a lake return at the Clive elevation would be longer than the fetch length for the Great Salt Lake. Second, the observed sedimentation patterns of the Great Salt Lake represent relatively short term dynamics of lakeshore processes – the dispersal area of sediments for the return of a lake at the Clive site and erosion of the embankment would likely develop over a timescale of multiple decades.

Google Earth© imagery was used to estimate alternative sediment dispersal areas using constraints from field observations of the distribution of conglomerate and sand deposits of the transgressive phase of Lake Bonneville. These estimations combined data from surface landforms and quarry-wall exposures of lake sediments at Clive.

Finally, alternative sediment dispersal patterns were estimated using Google Earth© imagery for Clive by centering the sediment dispersal at the Clive embankment and adjusting the dispersal patterns for the topographic features of the Clive area.

The following percentiles were assigned to the composite data to establish a distribution for the sediment dispersal parameter:

- 1%: 4 km^2 from smallest measured dispersal area
- 5%: 10 km^2 assuming only west-east wind directions
- 15%: 15 km^2 averaging dispersal areas for no longshore drift

- 30%: 16 km^2 averaging dispersal areas for N-S and SW-NE longshore drift
- 50% 24 km^2 assuming multidirectional winds and longshore drift
- 75% 36 km^2 averaging all single direction longshore drift dispersal areas

  95% 55 km^2 from maximum measured dispersal area

A gamma distribution was used to fit the percentages above, with mean of 24.2332 and standard deviation of 11.43731. A typical probability density function of this distribution is shown in Figure 12.

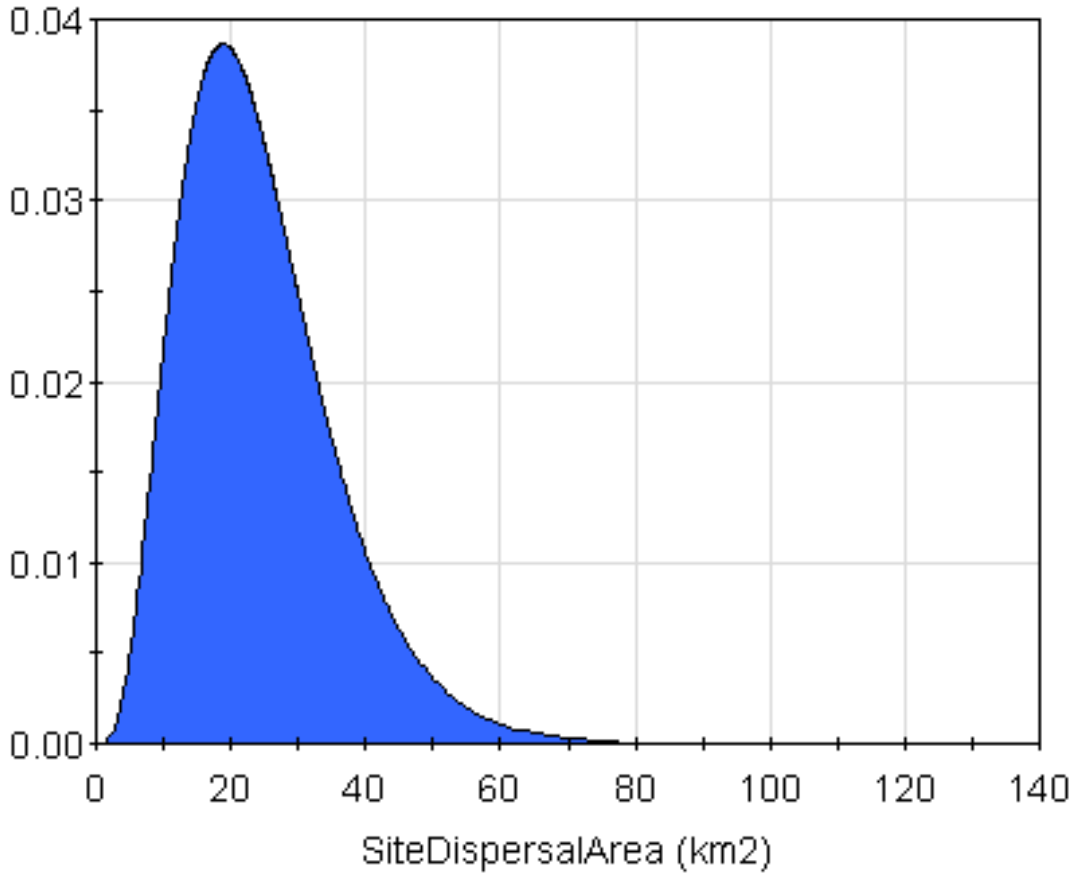

Figure 12. Probability density function for the area over which the waste embankment is dispersed upon destruction

7.7 Radionuclide Concentration in DU Waste

After a lake recedes, radionuclides in the original DU waste disposal volume are not likely to move to the surface in any significant amounts via diffusion or other processes. This section discusses processes that are likely to occur in deep time relating to the original DU waste source.

Infiltration rates will increase over time, moving material downward via advection, counteracting potential upward diffusion of radionuclides. The climate will become cooler and wetter, entering a glacial period, resulting in the lake return. Estimates of future net infiltration at Clive are supported by work for the Yucca Mountain Project. Faybishenko (2006) developed models predicting infiltration rates for future climate states based on factors including predicted precipitation, evapotranspiration, and temperature. The meteorological stations at Simpson and Spokane in Faybishenko (2006, Table 3) provide a reasonable range of infiltration rates for Clive of 40 mm/yr to 73 mm/yr, for a glacial phase.

An external, finely-discretized GoldSim model was used to test diffusion behavior at Clive, along with higher infiltration rates. The model results showed that if infiltration increased even to 10 mm/yr, downward advection would dominate upward diffusion in the model. Infiltration of 40 mm/yr to 73 mm/yr would move radionuclides that had diffused above the original grade back below grade.

Dry periods during the inner-glacial timeframes would be expected to behave like current conditions. Because of the uncertain nature of the deep time future conditions and timing and because it is important to keep the Deep Time Model simple, it was assumed that until the first lake returns, radionuclides migrate upwards via the processes of diffusion and plant and animal transport and that the associated material and radionuclides above grade is spread across the site dispersal area and is available to diffuse into an intermediate or deep lake. These simplifying assumptions ignore increases in infiltration during wetter periods in the climate cycle, which is a conservative approach.

7.8 Radionuclide Concentration in Sediment

The radioactivity per unit volume of sediment following the dispersal of the waste is estimated using Equation 13 below.

The model calculates radioactivity by volume in the sediment layers, after the embankment has been destroyed. The current implementation always mixes sediment with the full amount of waste, and does not consider a mixing depth; i.e., the waste is always fully mixed and not covered by sediment. Thus, radioactivity concentration in sediment is initially calculated under the assumption that all of the waste in the waste embankment is mixed evenly with the sediment that forms as a result of the lake destroying the embankment.

Concentration in sediment is initially calculated under the assumption that all of the waste that was above grade in the waste embankment is mixed evenly with the sediment that forms with the lake that destroys the embankment.

$$C_{\text{sediment}} = \frac{R_{\text{embankment}}}{V_{\text{material above grade}} + V_{\text{sediment}}}. \quad (13)$$

where

$R_{\text{embankment}}$	is all remaining radioactivity in the embankment,
$V_{\text{material above grade}}$	is the volume of material in the above grade portion of the embankment (estimated as 3,231,556 m^3), and
V_{sediment}	is calculated as the depth of sediment due to lake processes multiplied by the area over which the waste is dispersed.

This calculation assumes that there is no loss of waste from the initial dispersal region. While this calculation is counter to the modeling of dissolution into the water column of the lake, a simplifying assumption is that all waste that dissolves into the lake precipitates back into the sediment upon recession of the lake.

The concentrations in sediment are modeled as constant, except for decay and ingrowth, until a new lake occurs. When a new lake occurs, the sedimentation associated with that lake is likely to mix with some portion of the top layer of existing sediment and leave the lower layers of the sediment buried beneath. However, for simplicity, a conservative approach is to mix all sediment that contains waste, effectively keeping some portion of the waste near-surface. The concentration is again the total radioactivity divided by the volume containing waste, but the volume that contains waste now has the additional volume of sediment associated with the current lake.

7.9 Radioactivity in Lake Water

When lake water is present, radionuclides will partition between the water phase and the solid phase depending on element-specific solubility and sorption properties. Radionuclides remaining in the pore water will then diffuse into the lake. The waste is likely to mix over a wide area of the lake, and many forms of the waste are likely to bind with carbonate ions in the water, ultimately precipitating into carbonate sediments. As a conservative assumption, upon recession of the lake, all waste is assumed to precipitate back into the *local* sediments, meaning that all radionuclides in the sediments are returned to the sediments when the lake regresses.

When a lake returns, the sediments are assumed to be fully saturated, and radionuclides are partitioned from the sediment to the pore water within the sediment using the same partitioning coefficients (K_d) used for other sedimentary soils in the model. An important difference between the assumptions for this model and the model for transport from the embankment in the 10-ky model is that the lake water is assigned a different solubility for uranium for the Deep Time Model. While solubilities for all other radionuclides remain the same, the solubility for uranium is reduced to that of U_3O_8 which is appreciably lower than other forms of uranium originally present in the waste. This change in solubility for uranium is adopted because it is expected that by the time the first lake returns, soluble uranium forms (UO_3) either will have been leached from the embankment into the shallow aquifer or will have been converted into U(IV), which is also very insoluble.

As radionuclides associated with the sediments dissolve into the pore water, they diffuse into the lake water using a constant flux model based upon Fick's first law, with the following assumptions:

- The concentration in sediment remains constant over the deep time period. The sediment concentration should in fact diminish over time if enough mass is migrated into the water, but for simplicity, the sediment concentrations are kept constant across time steps.
- The diffusion length from the radionuclides in the sediment diffusing into the lake is about 0.5 m. This diffusive length value assumes the mixing depths of the sediment correspond to diffusive processes from the sediment into the lake.
- Mixing depths are expected to be between 0 and 1 m, with 0.5 m being most likely. The distribution was set up as a normal distribution with mean of 0.5 m and standard deviation of 0.16 m so that 99% of the distribution will be between 0 and 1 m. The distribution is truncated at 0 m so that no negative diffusion lengths are chosen.

Fick's law for this case estimates the mass diffusing from a given volume of sediment into the lake with time. The mass (or activity) per area per time is the flux. Fick's law states that this flux is given by the difference in mass concentration over a distance (the concentration gradient) multiplied by a free-water diffusion coefficient, across a diffusive area. The calculation assumes that there is a stagnant interface boundary layer of water between the sediment and the open water that is the thickness of the diffusion length (~0.5 m). The assumption is also made that the mass concentration is zero in the open water. The difference in concentration across the stagnant layer is then the concentration in the sediment C_v minus the concentration in the open water or C_v – 0 g/mL. Fick's law applied to diffusion is used to define the mass (or activity) flux J:

$$J = \frac{R}{\Delta t\, A} = D_m \frac{C_v}{b_{bdy}}. \tag{14}$$

where

R is the mass (M) activity (T^{-1}),

ΔT is the length of the time period (T),

A is the area of the sediment that contains the waste (L^2),

D_m is the diffusion coefficient for the radionuclide in water (L^2/T), and

b_{bdy} is the thickness of the boundary layer.

Multiplying both sides of the equation by $\Delta T \cdot A$ gives

$$R = \Delta T \cdot D_m \cdot \frac{C_V}{0.1\ \text{m}} \cdot A. \tag{15}$$

Concentration in lake water is calculated based upon the conservative assumption that the radioactive material does not dilute in a large basin of the lake but rather remains in the water column immediately above the dispersed area. The activity concentration in the lake water is then calculated by dividing the total activity, R, by the volume of lake water. The volume of lake water is the product of the lake depth and the dispersal area:

$$C_v = \frac{R}{D \cdot A} \tag{16}$$

where

C_v is concentration (M/L^3 or T^{-1}/L^3),

R is the mass (M) or radioactivity (T^{-1}),

A is the area of the sediment that contains waste (the dispersed area, as L^2), and

D is the depth of the lake (L).

There is an insufficient record of lake elevations to construct a data-based distribution for lake depth. Thus, the distributions for lake depth are chosen based upon the conceptual model. Depths for intermediate lakes have a Beta distribution with mean of 30 m, standard deviation 18 m, minimum of 0 m, and maximum of 100 m. Depths for deep lakes have a Beta distribution with mean 150 m, standard deviation 20 m, minimum of 100 m, and maximum of 200 m.

For intermediate lakes, the time step is about the duration of the intermediate lake. For deep lakes, the lake may exist for several time steps in the GoldSim model, in which case the time step is the portion of the time step for which the lake is present. When deep lakes cross multiple time steps, the concentration in sediment is allowed to change between time steps (only due to decay and ingrowth) and the activity in the lake water is accumulated over those time steps.

7.10 Modeling of ^{222}Rn Flux

Radon-222 flux through the overlying sediment is calculated using the approach described in the Nuclear Regulatory Commission (NRC) Regulatory Guide 3.64 *Calculation of Radon Flux Attenuation by Earthen Uranium Mill Tailings Covers* (NRC, 1989). These equations were developed for estimating radon flux from uranium mill tailings buried under a monofill cover. For the Deep Time Model, an assumption is made that the material above the below-grade DU waste and the additional lake sedimentation is homogenous material with properties similar to those of the surrounding Unit 3 sediments. The use of an analytical model such as that described in NRC (1989) allows radon flux to be estimated through a homogeneous cover of varying thickness with minimal complexity.

The increasing depth of material covering the disposed DU waste over time will result in attenuation of radon flux. However, this rate of attenuation will be partly offset by the slowly increasing activity of the radioactive progeny of ^{238}U. Previous modeling results, such as those from the Clive DU PA Model v1.2, indicated that sediment accumulation overwhelms the influence of progeny ingrowth.

Although the median and mean sediment thickness track closely, the mean radon ground surface flux is much larger than the median. This strongly skewed result for radon flux is a consequence of the non-linearities inherent in the NRC radon ground surface flux calculation. These are equations (9) through (12) in NRC (1989):

$$J_t = 10^4 R_t \rho_t E_t \sqrt{\lambda D_t} \tanh\left(x_t \sqrt{\lambda / D_t}\right)$$

$$b_t = \sqrt{\lambda / D_t}, \quad b_c = \sqrt{\lambda / D_c}$$

$$a_t = n_t^2 D_t [1 - (1-k) m_t]^2, \quad a_c = n_c^2 D_c [1 - (1-k) m_c]^2 \tag{17}$$

$$J_c = \frac{2 J_t e^{(-b_c x_c)}}{1 + \sqrt{a_t / a_c} \tanh(b_t x_t) + \left[1 - \sqrt{a_t / a_c} \tanh(b_t x_t)\right] e^{(-2 b_c x_c)}}$$

The definitions of variables are available in the NRC Regulatory Guide (1989), but the salient point is that these equations will produce a highly non-linear result, J_c, which is the ground surface flux of radon. Although all of the inputs to the calculation are essentially normal distributions, the division calculations, exponents, etc. in the equations produce non-linear results.

Modeling of radon transport to the surface of the intact Federal DU Cell in the Clive DU PA Model v1.2 does not lend itself to such simplified analytical solutions, because the cover is constructed of layers with widely-varying properties. Radon diffusive flux is therefore integrated with other transport processes employing a column of well-mixed cells, allowing for the vertical redistribution of radionuclides over time throughout the disposal system by diffusive, advective, and biotic processes. Because the above-ground part of the Federal DU Cell is assumed to be dispersed by wave action from the first intermediate lake, these processes are not relevant to the Deep Time Model except insofar as they affect radionuclide concentrations in the below-grade waste cells.

7.10.1 Waste and Sediment Water Content

Volumetric water contents are defined for the DU waste, and for sediments overlying the waste, in order to support radon diffusive flux calculations through these sediments.

In the 10,000-year model, the waste material is assumed to be Unit 3 material. In the Deep Time Model it is also assumed to be Unit 3, for both the mound material that is directly above the waste but below grade when the first lake returns and for the sediment material that is deposited from deep and intermediate lakes in deep time. Sediment porosity is assumed to be the same as Unit 3 porosity.

The Deep Time Model water contents for the cover materials after the first lake recedes are based on concentrations of waste materials just above the DU waste, in Waste Cells 17 – 21 and the upper-most waste cell containing DU waste, Waste Cell 22. This cell may not be completely full of DU waste, because the discretization of the model may not match exactly the discretization of the disposed wastes, so Cell 22 was included in these calculations for moisture content. Because the Deep Time Model is now fully integrated in the v1.4 model, these values are taken directly from the waste properties and align with those directly for each model realization.

7.11 Human Health Exposure and Dose Assessment

In the Deep Time component of the GoldSim model, external radiation dose and radon inhalation dose are evaluated for the time period after a lake returns. Specifically, this special analysis evaluates dose at a time immediately after the first intermediate lake has formed and subsequently receded. The wave action of the lake is assumed to have destroyed the embankment. The DU wastes at this point in time when the intermediate lake has receded are covered by a thickness of material equal to the thickness of the eolian sediments that have been continually deposited at a constant rate over time, plus the deposition of lake sediments while the intermediate lake exists. The lower stratum of material of thickness equivalent to the eolian sediments is comprised of the waste layers that existed above the DU waste in the embankment. Although these wastes at one time contained radionuclides that had migrated upwards from the DU, these radionuclides are assumed to have been dissolved and dispersed during the time when the intermediate lake was present. Therefore, both these materials as well as the lacustrine sediments are assumed to be practically free of DU-related radionuclides in this modeling.

The purpose of the dose calculations the Deep Time component of the GoldSim model is to determine whether hypothetical doses in Deep Time may be higher or lower than doses calculated for the 10,000-year performance period. The Deep Time dose calculation results are not considered to have independent validity. Rather, they are a tool for evaluating the relative radiation dose during these two time periods. For the dose assessment during the first 10,000 years of the Clive DU PA v1.4 Model, two future use exposure scenarios are identified for the Clive site: ranching and recreation. However, only ranching receptors are evaluated for the Deep Time component of the model because their utilization of the area including the Clive site is far greater than that of recreational users and their doses are therefore higher.

The radiological assessment method for the Deep Time the Deep Time component of the GoldSim model calculates total effective dose equivalent (TEDE) as the product of exposure (behavioral) parameters, dose conversion factors (DCFs), and the concentrations of radium and gamma-emitting radionuclides in the DU waste. The calculations are analogous to those described for the Ranching scenario during the 10,000-year performance period with two exceptions:

1. Radon flux is calculated using the approach described in the Nuclear Regulatory Commission (NRC) Regulatory Guide 3.64 *Calculation of Radon Flux Attenuation by Earthen Uranium Mill Tailings Covers* (NRC, 1989). These equations were developed for estimating radon flux from uranium mill tailings buried under a monofill cover, and the properties of the overlying materials are homogenous material with properties similar to those of the surrounding Unit 4 sediments.
2. The external DCFs are multiplied by radionuclide-specific modifying factors to account for the attenuation of external gamma radiation due to the material that overlies the DU waste. The modifying factors were calculated using the RESRAD computer code by evaluating the ratio of external dose at different cover thicknesses to external dose with no overlying material.

8.0 References

Adams, K.D., 2003, Age and paleoclimatic significance of late Holocene lakes in the Carson Sink, NV, USA, *Quaternary Research*, Vol. 60, pp. 294–306, 2003.

Archer, D. and A. Ganopolski, 2005. A movable trigger: fossil fuel CO_2 and the onset of the next glaciation. *Geochemistry, Geophysics, Geosystems*, 6(5), doi:10.1029/2004GC000891.

Asmerom, Y., Polyak, V. J., and S. J. Burns, 2010. Variable winter moisture in the southwestern United States linked to rapid glacial climate shifts. *Nature Geoscience*, 3, 114-117.

Balch D.P., A.S. Cohen, D.W. Schnurrenberger, B.J. Haskell, B.L.V. Garces, J.W. Beck, H. Cheng, and R.L. Edwards, 2005. Ecosystem and paleohydrological response to Quaternary climate change in the Bonneville basin, Utah, *Palaeogeography, Palaeoclimatology, Palaeoecology*, Vol. 221, pp. 99–121.

Berger, A., 1988. Milankovitch theory and climate. *Reviews of Geophysics*, 26(4): 624-657.

Berger, A. and M. F. Loutre, 2002. An exceptionally long interglacial ahead? *Science*, 297: 1287-1288.

Benson, L.V., S.P. Lund, J.P. Smoot, D.E. Rhode, R.J. Spencer, K.L. Verosub, L.A. Louderback, C.A. Johnson, R.O Rye, R.M. Negrini, 2011, *The Rise and Fall of Lake Bonneville Between 45 and 10.5 ka,* Quaternary International, Vol. 235, p. 57-69.

Briggs, R.W., S.G. Wesnousky, and K.D. Adams, 2005, Late Pleistocene and late Holocene lake highstands in the Pyramid Lake subbasin of Lake Lahontan, Nevada, USA, *Quaternary Research,* Vol. 64, pp. 257–263, 2005.

Brimhall W. H. and L. B. Merritt, 1981. The geology of Utah Lake – implications for resource management. *Great Basin Naturalist Memoirs*, 5: 24-42.

Brockwell, P.J. and R.A. Davis, 1991. *Time Series: Theory and Methods*. Springer-Verlag, New York, NY.

Clark, P. U., Dyke, A. S., Shakun, J. D., Carlson, A. E., Clark, J., Wohlfarth, B., Mitrovica, J. X., Hostetler, S. W., and A. M. McCabe, 2009. The Last Glacial Maximum. *Science*, 325: 710-714.

Cochelin, Anne-Sophie B., L.A. Mysak, Z. Wang, 2006, Simulation of long-term future climate changes with the green McGill paleoclimate model: The next glacial inception. *Climate Change,* 79, 381-401.

Cook, E.R., R. Seager, R.R. Helm Jr, R. S. Vose, C. Herweijer, and C. Woodhouse, 2010. Megadroughts in North America: Placing IPCC Projection of Hydroclimatic Change in a Long-Term Palaeoclimate Context, *Journal of Quaternary Science,* 25, Issue 1, 48-61.Currey, D.R., G. Atwood, and D.R. Mabey, *Map 73 Major Levels of Great Salt Lake and Lake Bonneville*, Utah Geological and Mineral Survey, Salt Lake City, UT, May 1984

Davis, O.K., 1998. Palynological evidence for vegetation cycles in a 1.5 million yr pollen record from the Great Salt Lake, Utah, *U.S.A.*, *Palaeogeography, Palaeoclimatology, Palaeoecology*, Vol. 138, pp. 175–185.

Driscoll, N. W. and G. H. Haug, 1998. A short circuit in thermohaline circulation: a cause for Northern Hemisphere glaciation. *Science*, 282: 436-438.

Einselle, G. and M. Hinderer, 1997. Terrestrial sediment yield and the lifetimes of reservoirs, lakes, and larger basins. *Geologische Rundschau*, 86: 288-310.

EPICA community members, 2004. Eight glacial cycles from an Antarctic ice core. *Nature*, 429: 623-628.

Faybishenko, B. 2006. Climatic Forecasting of Net Infiltration at Yucca Mountain Using Analouge Meteorological Data. Lawrence Berkeley National Laboratory. DT#46762 QA:NA. MOL.20061204.0226.

Fritz, S.C., 1996, Paleolimnological records of climatic change in North America, *Limnol. Oceanogr.* 45, 882-889.

GTG (GoldSim Technology Group), 2011. *GoldSim: Monte Carlo Simulation Software for Decision and Risk Analysis*, http://www.goldsim.com

Harding, B.L., A.W. Wood, and J.R. Prarie, 2012. The Implications of Climate Change Scenario Selection for Future Streamflow Projection in the Upper Colorado River Basin, *Hydrol. Earth Syst. Sci, 16, 3989-4007.*

Hart, W. S., Quade, J., Madsen, D. B., Kaufmann, D. S., and C. G. Oviatt, 2004. The $^{87}Sr/^{86}Sr$ Ratios of Lacustrine Carbonates and Lake-level History of the Bonneville Paleolake System. *GSA Bulletin*, 116: 1107-1119.

Haug, G. H. and R. Tiedemann, 1998. Effect of the Formation of the Isthmus of Panama on Atlantic Ocean Thermohaline Circulation. *Nature*, 393: 673-676.

Hays, J. D., Imbire, J., and N. J. Shackleton, 1976. Variations in the Earth's Orbit: Pacemaker of the Ice Ages. *Science*, 194: 1121-1132.

IAEA. The Safety Case and Safety Assessment for the Disposal of Radioactive Waste. Vienna, Austria: International Atomic Energy Agency; Specific Safety Guide No. SSG-23; 2012.Jansen, E. J. Overpeck, K.R. Briffa, J.-C. Duplessy, F. Joosv, V. Masson-Delmotte, D. Olago, B. Otto-Bliesner, W.R. Peltier, S. Rahmstorf, R. Ramesh, D.. Raynaud, D. Rind, O. Solomina, R. Villalba, and D. Zang, 2007, Palaeoclimate. In: *Climate Change 2007: The Physical Science Basis. Contribution of Working Group I to the fourth Assessment Report of the Intergovernmental Panel on Climate Change* [Solomon, s. D. Qin, M. Manning, Z. Chen, M. Marquis, K.B. Averyt, M. Tigor and H.L Miller (eds.)] Cambridge University Press, Cambridge, United Kingdom and New York, NY, USA.

Jewell, P.W. 2010, River incision, circulation, and wind regime of Pleistocene Lake Bonneville, USA, *Palaeogeography, Palaeoclimatology, Palaeoecology,* 293, 41-50.

Jewell, P.W., and K. Nicoll, Wind Regimes and Eolian Transport in the Great Basin, U.S.A., Geomorphology 129, 1-13 (2011).

Jouzel, J., Masson-Delmotte, V., Cattani, O., Dreyfus, G., *et al.*, 2007. Orbital and millennial Antarctic climate variability over the past 800,000 yr. *Science*, 317: 793-796.

Kukla, G. J., R. K. Matthews, J. M. Mitchell Jr., *Quat. Res.* **2**, 261 (1972)

Lisiecki, L. E. and M. E. Raymo, 2005. A Pliocene-Pleistocene stack of 57 globally distributed benthic $\delta^{18}O$ records. *Paleoceanography*, 20, PA1003, doi:10.1029/2004PA001071.

Link, P. K., Kaufmann, D. S., and Thackray, G. D., 1999. Field guide to Pleistocene lakes Thatcher and Bonneville and the Bonneville flood, southeastern Idaho, *In*: Hughes S. S. and G. D Thackray (eds.), *Guidebook to the Geology of Eastern Idaho*, Idaho Museum of Natural History, p. 251-266.

Lyle, M., L. Heusser, C. Rovelo, M. Yamamoto, J. Barron, N.S. Diffenbaugh, T. Herbert, D. Andreasen, 2012, Out of the Tropics: The Pacific, Great Basin Lakes, and Late Pleistocene Water Cycle in the Western United States, *Science*, Vol. 337, p. 1629–1633.

Machette, M.N., S.F. Personius, and A.R. Nelson, 1992. Paleoseismology of the Wasatch fault zone: A summary of recent investigations, interpretations, and conclusions, in Gori, P.L., and W.W. Hays, eds., *Assessment of regional earthquake hazards and risk along the Wasatch Front, Utah,* U.S. Geological Survey Professional Paper 1500-A-J, pp. A1–A71, 1992.

Madsen, D.B., 2000. *Late Quaternary Paleoecology in the Bonneville Basin,* Utah Geological Survey Bulletin 130, 2000.

Masson-Delmotte, V., Stenni, B., Pol, K., Braconnot, P., *et al.*, 2010. EPICA Dome C record of glacial and interglacial intensities. *Quaternary Science Reviews*, 29: 113-128.

Masson-Delmotte, V., M. Schulz, A. Abe-Ouchi, J. Beer, A. Ganopolski, J.F. Gonzalez Rouco, E. Jansen, K. Lambeck, J. Luterbacher, T. Naish, T. Osborn, B. Otto-Bliesner, T. Quinn, R.. Ramesh, M. Rojas, X. Shao, and A. Timmermann, 2013, Information from Paleoclimate Archive. In: *Climate Change 2013: The Physical Science Basis. Contribution of Working group I to the Fifth Assessment Report of the Intergovernmental Panel on Climate Change,* Stocker, T.F., D. Qin, G.-K. Plattner, M. Tignor, S.K. Allen, J. Boschung, A. Nauels, Y. Xia, V. Bex and P.M. Midgley (eds.)]. Cambridge University Press, Cambridge, United Kingdom and New York, NY, USA.

Matsubara, Y. and A. D. Howard, 2009. A spatially explicit model of runoff, evaporation, and lake extent: application to modern and late Pleistocene lakes in the Great Basin region, western United States. *Water Resources Research*, 45, W06425, doi:10.1029/2007WR005953.

Miller, D.M., C.G. Oviatt, and J.P. Mcgeehin, 2013. Stratigraphy and chronology of Provo shoreline deposits and lake-level implications, Late Pleistocene Lake Bonneville, eastern Great Basin, U.S.A., *Boreas*, Vol. 42, pp. 342–361, 2013.

Nash, W.P., 1990, *Black Rock Desert, Utah,* in C.A Woods and J. Kienle, eds. Volcanoes of North America, Cambridge University Press, Cambridge p. 271-273.

Nelson, D.T., 2012. Geomorphic and Stratigraphic Development of Lake Bonneville's Intermediate Paleoshorelines during the Late Pleistocene, PhD Dissertation, University of Utah, 237 p.

Neptune and Company, Inc., 2015a, *Neptune field studies, December, 2014, Eolian depositional history Clive Disposal Site*.

Neptune and Company, Inc., 2015b, *Final report the Clive DU PA Model*, Clive DU PA Model v1.4, Neptune and Company In., (November, 2015).

NRC (Nuclear Regulatory Commission), 1989. *Calculation of Radon Flux Attenuation by Earthen Uranium Mill Tailings Covers*, U.S. Nuclear Regulatory Commission, Office of Nuclear Regulatory Research, Task WM 503-4, June 1989.

Oviatt, C. G. and W. P. Nash, 1989. Late Pleistocene basaltic ash and volcanic eruptions in the Bonneville basin, Utah. *Geological Society of America Bulletin*, 101: 292-303.

Oviatt, C. G., McCoy, W. D., and Nash, W. P., 1994a. Sequence stratigraphy of lacustrine deposits: a Quaternary example from the Bonneville basin, Utah. *Geological Society of America Bulletin,* 106: 133-144.

Oviatt, C.G., G.D. Habiger and J.E. Hay, 1994b. *Variation in the Composition of Lake Bonneville Marl: A Potential Key to Lake-Level Fluctuations and Paleoclimate,* Journal of Paleolimnology, Vol 11, p. 19-30.

Oviatt, C. G., 1997. Lake Bonneville fluctuations and global climate change. *Geology*, 25(2): 155-158.

Oviatt, C. G., Thompson, R. S., Kauffman, D. S., Bright, J., and R. M. Forester, 1999. Reinterpretation of the Burmester core, Bonneville Basin, Utah. *Quaternary Research*, 52: 180-184.

Oviatt, C.G., 2002, *Comparing the Shoreline and Offshore Sedimentary Records of Lake Bonneville*. Abstracts with Programs - Geological Society of America 34(6): 292.

Oviatt, C. G., D. M. Miller, J. P. McGeehin, C. Zachary, and S. Mahan, 2005. The Younger Dryas phase of Great Salt Lake, Utah, USA, *Palaeogeography, Palaeoclimatology, Palaeoecology*, 219: 263-284.

Oviatt, C.G., and B. P. Nash, 2014, *The Pony Express Basaltic Ash: A Stratigraphic Marker in Lake Bonneville Sediments, Utah,* Miscellaneous Publication 14-1, Utah Geological Survey 10 p.

Oviatt, C.G., *Chronology of Lake Bonneville, 30,000 to 10,000 yr B.P*. Quaternary Science Reviews 110, 166-171, (2015).

Paillard, D., 2001. Glacial cycles: toward a new paradigm. *Reviews of Geophysics*, 39(3): 325-346.

Paillard, D., 2006. What drives the Ice Age cycle? *Science*, 313: 455-456.

Ruddiman, W.F., 2006. Orbital Changes and Climate, Quaternary Science Reviews, Vol. 25, pp. 3092–3112.Sack, D., 1999.The composite nature of the Provo Level of Lake Bonneville, Great Basin, Western North America, *Quaternary Research*, v. 52, 316-327.

SC&A, Inc. 2015. Safety Evaluation Report: Volume I. *for* Utah Department of Environmental Quality. April 2015.

Schnurrenber, D. J. Russell, and K Kelts, 2003, Classification of lacustrine sediments based on sedimentary components, Journal of Paleolimnology *29, p. 141-154.*

Schofield, I., P. Jewell, M. Chan, D. Currey, and M. Gregory, 2004, Shoreline development, longshore transport, and surface water dynamics, Pleistocene Lake Bonneville, Utah, *Earth Surf. Process. Landforms*, 29, 167-1690.

Tzedakis, P.C., E.W. Wolff, L.C. Skinner, V. Brovkin, d.A. Hodell, J.F. McManus, and D. Raynaud, 2012a, Can we predict the duration of an interglacial? *Climate Past 8, 1473-1485.*

Tzedakis, P.C., J.E.T. Channel, D.A. Hodell, H.F. Kleiven, and L.C. Skinner, 2012b, Determining the natural length of the current interglacial, *Nature Geoscience*, 5, 138-141.

United States Geological Survey (USGS), 2001. National Water Information System data (Water Data for the Nation), accessed December, 2010 URL: http://waterdata.usgs.gov

Utah, State of, 2015, Utah Administrative Code Rule R313-25. License Requirements for Land Disposal of Radioactive Waste - General Provisions. As in effect on September 1, 2015. (http://www.rules.utah.gov/publicat/code/r313/r313-025.htm, accessed 5 Nov 2015).

Woodhouse, C.A., D. M. Meko, G. M. MacDonald, D.W. Stahle, and E. R. Cook, 2010. A 1,200-year Perspective of 21st Century Drought in Southwestern North America, *Proc. Natl. Acad. Of Sciences*, 107, 21283-21288.

Appendix A

A.1 Clive Pit Wall Interpretation (C. G. Oviatt, unpublished data) and stratigraphic comparison with quarry wall studies from Neptune (2015a).

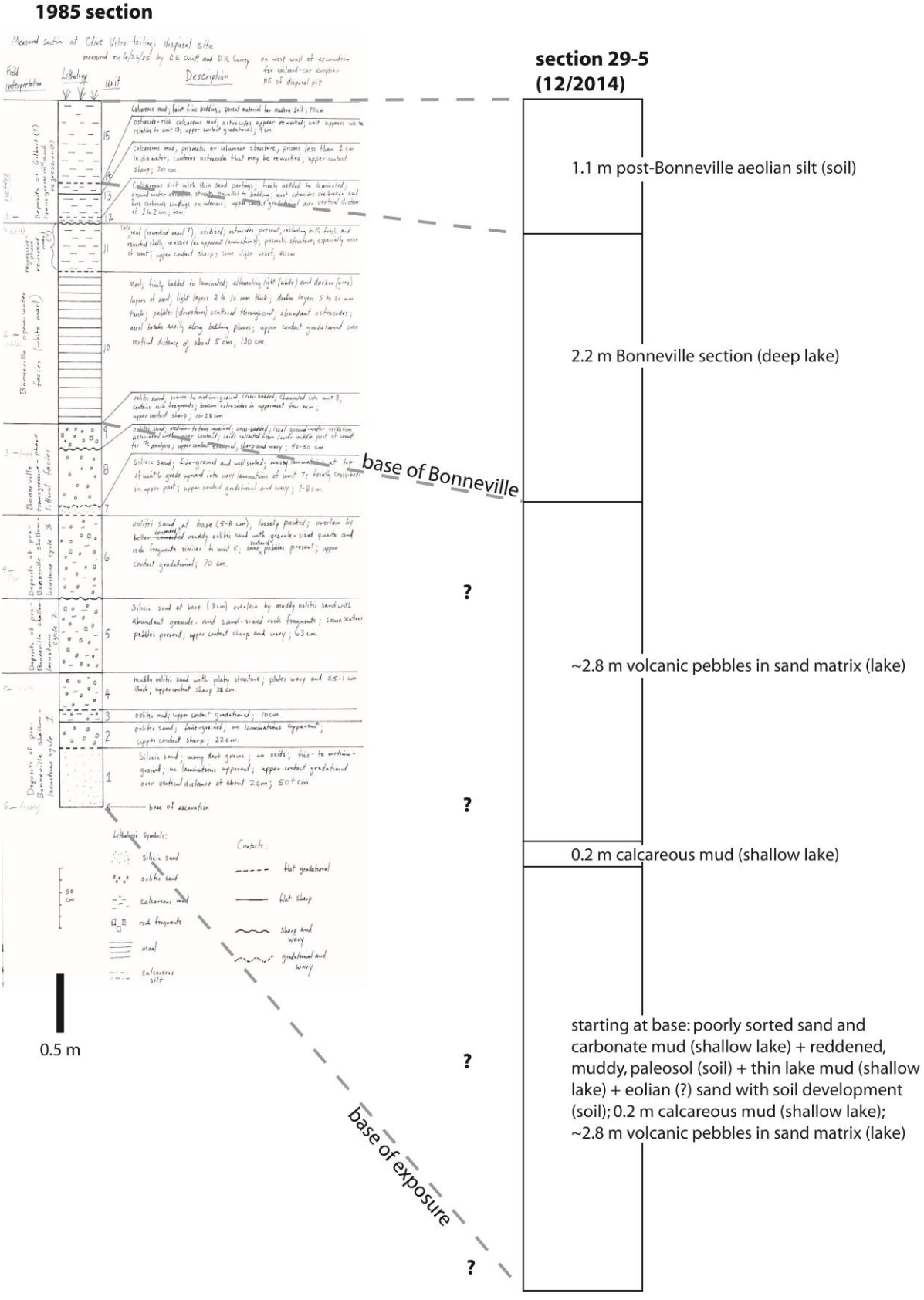
1985 section
section 29-5
(12/2014)
1.1 m post-Bonneville aeolian silt (soil)
2.2 m Bonneville section (deep lake)
base of Bonneville
~2.8 m volcanic pebbles in sand matrix (lake)
0.2 m calcareous mud (shallow lake)
starting at base: poorly sorted sand and carbonate mud (shallow lake) + reddened, muddy, paleosol (soil) + thin lake mud (shallow lake) + eolian (?) sand with soil development (soil); 0.2 m calcareous mud (shallow lake); ~2.8 m volcanic pebbles in sand matrix (lake)
base of exposure
?
?
?
0.5 m

Appendix B

B.1 Knolls Core Interpretation (C. G. Oviatt, unpublished data)

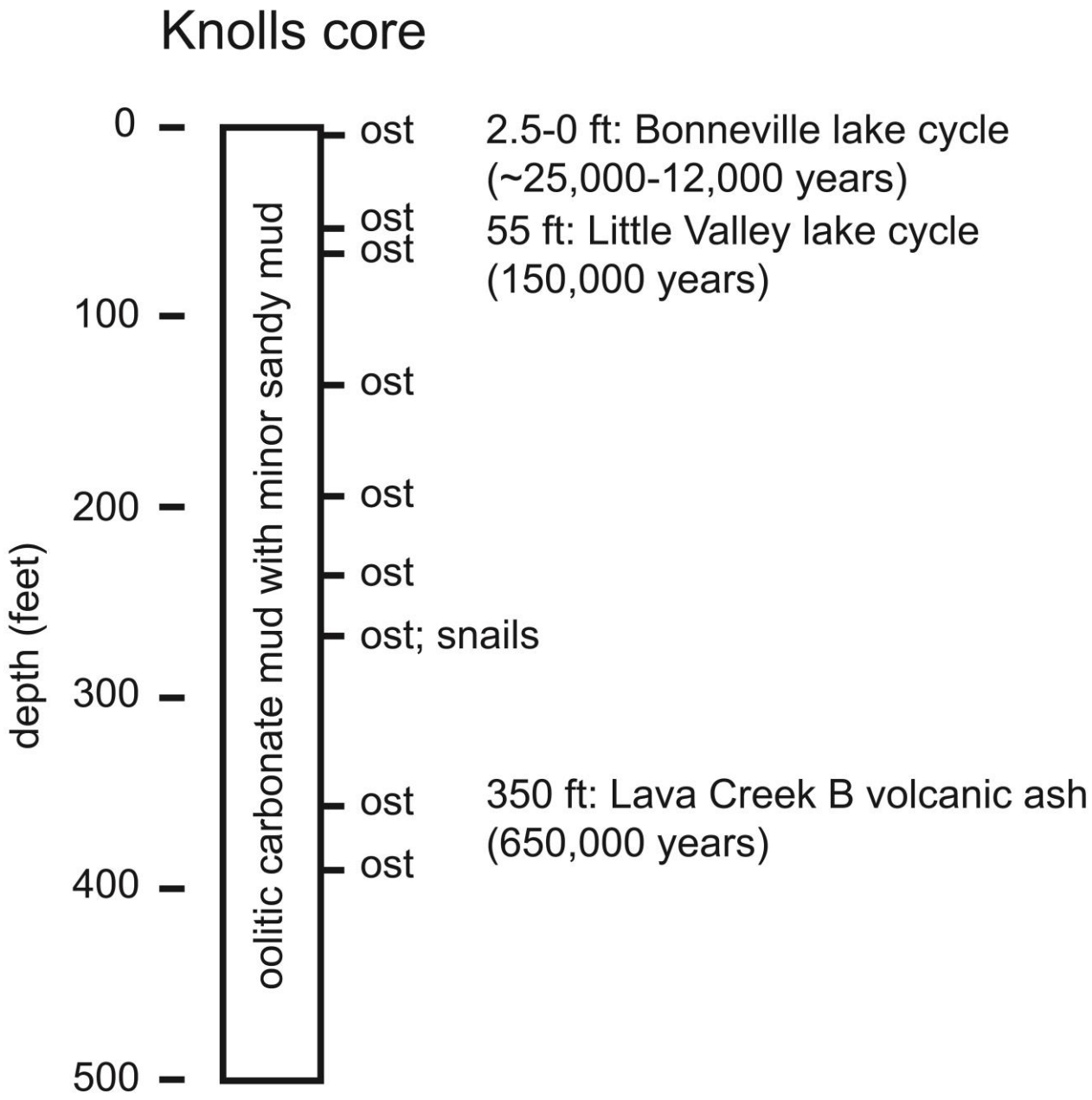

ost = ostracodes (fresh water of a lake or marsh)
snails indicate shallow fresh water